



THE BOUNDARY COLLOCATION METHOD WITH MESHLESS CONCEPT FOR ACOUSTIC EIGENANALYSIS OF TWO-DIMENSIONAL CAVITIES USING RADIAL BASIS FUNCTION

J. T. CHEN, M. H. CHANG, K. H. CHEN AND S. R. LIN

*Department of Harbor and River Engineering, National Taiwan Ocean University, 202 Keelung,
Taiwan, Republic of China. E-mail: jtchen@mail.ntou.edu.tw*

(Received 30 July 2001, and in final form 8 January 2002)

In this paper, a meshless method for the acoustic eigenfrequencies using radial basis function (RBF) is proposed. The coefficients of influence matrices are easily determined by the two-point functions. In determining the diagonal elements of the influence matrices, two techniques, limiting approach and invariant method, are employed. Based on the RBF in the imaginary-part kernel, the method results in spurious eigenvalues which can be separated by using the singular value decomposition (SVD) technique in conjunction with the Fredholm alternative theorem. To understand why the spurious eigenvalues occur, analytical study in the discrete system by discretizing the circular boundary is conducted by using circulants. By using the SVD updating terms and documents, the true and spurious eigensolutions can be extracted out respectively. Several examples are demonstrated to see the validity of the present method.

© 2002 Elsevier Science Ltd. All rights reserved.

1. INTRODUCTION

The mesh generation of a complicated geometry is time consuming in the stage of model creation for engineers in dealing with the engineering problems by using the numerical methods, such as the finite difference method (FDM), finite element method (FEM) and boundary element method (BEM). In the recent years, researchers have paid attention to the meshless method which the element is free. The initial idea of meshless method dates back to the smooth particle hydrodynamics (SPH) method for modelling astrophysical phenomena [1]. Several meshless methods have also been reported in the literature, for example, the element-free Galerkin method [2] and the reproducing kernel method [3].

For acoustics, the integral equations have been utilized to solve the interior and exterior problems for a long time. Several approaches, e.g., complex-valued boundary element method [4], multiple reciprocity method (MRM) [5–7], and the real-part boundary element method [5, 8] have been developed for acoustic problems. To solve acoustic problems by using the complex-valued BEM, the influence coefficient matrix would be complex arithmetics [9, 10]. Therefore, Tai and Shaw [11] employed only the real-part kernel to solve the eigenvalue problems and to avoid the complex-valued computation. The computation of the real-part kernel method or the MRM [11, 12] has some advantages, but it still faces both the singular and hypersingular integrals. To avoid the singular and hypersingular integrals, De Mey [13] used imaginary-part kernel to solve the eigenvalue

problems. At the same time, De Mey also found the spurious eigensolutions but he did not discuss them analytically. Kang *et al.* [14–16] proposed the non-dimensional dynamic influence function (NDIF) method to solve the eigenproblem of an acoustic cavity. Later, Chen *et al.* [17] commented that the NDIF method is a special case of imaginary-part BEM. Nevertheless, spurious eigensolutions are inherent in the imaginary-part BEM, real-part BEM and MRM. Numerically speaking, the spurious eigensolutions result from the rank deficiency of the coefficient matrix which is less than $2N$, where $2N$ is the number of boundary unknowns. This implies the fewer number of constraint equations making the solution space larger. Mathematically speaking, the spurious eigensolutions for interior acoustics and fictitious solutions for exterior acoustics arise from an “improper approximation of the null space of operator”.

In this paper, we will employ the imaginary-part kernel to solve the acoustic eigenproblems. In solving the problem numerically, elements are not required and only boundary nodes are necessary. Both the collocation and source points are distributed on the boundary only. Besides, the kernel function is composed of two-point function which is a kind of radial basis function. To examine the reason why spurious eigenvalues occur in the above methods, we will employ the SVD updating technique in conjunction with the Fredholm alternative theorem to overcome this difficulty by assembling the dual equations [18–20]. The SVD updating terms and updating documents will be employed to extract out the true and spurious eigenvalues for two-dimensional cavities respectively. For a special case of circular cavity, the spurious eigensolutions will be analytically predicted in the discrete system of circulants. Finally, the true eigenvalues for a circular cavity will be derived analytically by approaching the discrete system to the continuous system using the analytical properties of circulants [21].

2. MESHLESS FORMULATION USING RADIAL BASIS FUNCTION OF THE IMAGINARY-PART KERNEL

The governing equation for an interior acoustic problem is the Helmholtz equation as follows:

$$(\nabla^2 + k^2)u(x_1, x_2) = 0, \quad (x_1, x_2) \in D, \quad (1)$$

where ∇^2 is the Laplacian operator, D is the domain of the cavity and k is the wave number which is angular frequency over the speed of sound. The boundary conditions can be either the Neumann or Dirichlet type.

The radial basis function is expressed by

$$G(x_i, s_j) = \varphi(|s_j - x_i|), \quad (2)$$

where x_i and s_j are the i th collocation and j th source points, respectively. The Euclidean norm $|s_j - x_i|$ is referred to as the radial distance between the collocation and source points. The two-point function ($\varphi(|s_j - x_i|)$) is called radial basis function since it depends on the radial distance between x_i and s_j . By considering the imaginary-part kernel of fundamental solution for the Helmholtz equation ($U(s, x) = \text{Im}\{iH_0^{(1)}(kr)\}$) with globally supported radial basis function, we can choose the four kernels in the dual formulation [5, 22],

$$U(s, x) = J_0(k|s - x|) = J_0(kr), \quad (3)$$

$$T(s, x) = \frac{\partial U(s, x)}{\partial n_s} = -k \frac{J_1(kr)y_i n_i}{r}, \quad (4)$$

$$L(s, x) = \frac{\partial U(s, x)}{\partial n_x} = k \frac{J_1(kr)y_j \bar{n}_j}{r}, \tag{5}$$

$$M(s, x) = \frac{\partial^2 U(s, x)}{\partial n_s \partial n_x} = k \left(\frac{-kJ_2(kr)y_i y_j n_i \bar{n}_j}{r^2} + \frac{J_1(kr)n_i \bar{n}_i}{r} \right), \tag{6}$$

where $r \equiv |s - x|$ is the distance between the source and collocation points; n_i is the i th component of the outnormal vector at s ; \bar{n}_i is the i th component of the outnormal vector at x , J_n denotes the first-kind Bessel function of the n th order, and $y_i \equiv s_i - x_i, i = 1, 2$. Based on the dual formulation [23] for the indirect method, we can represent the acoustic field solution by

Single-layer potential approach:

$$u(x_i) = \sum_j U(s_j, x_i) \phi_j \xrightarrow{\text{matrix form}} \{u_i\} = [U_{ij}] \{\phi_j\}, \tag{7}$$

$$t(x_i) = \sum_j \frac{\partial U(s_j, x_i)}{\partial n_x} \phi_j \xrightarrow{\text{matrix form}} \{t_i\} = [L_{ij}] \{\phi_j\}. \tag{8}$$

Double-layer potential approach:

$$u(x_i) = \sum_j T(s_j, x_i) \psi_j \xrightarrow{\text{matrix form}} \{u_i\} = [T_{ij}] \{\psi_j\}, \tag{9}$$

$$t(x_i) = \sum_j \frac{\partial T(s_j, x_i)}{\partial n_x} \psi_j \xrightarrow{\text{matrix form}} \{t_i\} = [M_{ij}] \{\psi_j\}, \tag{10}$$

where $\{\phi_j\}$ and $\{\psi_j\}$ are the generalized unknowns by using the single- and double-layer potential approaches respectively. By adopting the two bases, $J_m(kx)$ and its derivative $J'_m(kx)$, we can decompose the imaginary-part kernel functions into the separate forms,

$$U(s, x) = \begin{cases} U^I(\theta, 0) = \sum_{m=-\infty}^{\infty} J_m(kR)J_m(k\rho)\cos(m\theta), & R > \rho, \\ U^E(\theta, 0) = \sum_{m=-\infty}^{\infty} J_m(k\rho)J_m(kR)\cos(m\theta), & R < \rho, \end{cases} \tag{11}$$

$$T(s, x) = \begin{cases} T^I(\theta, 0) = \sum_{m=-\infty}^{\infty} kJ'_m(kR)J_m(k\rho)\cos(m\theta), & R > \rho, \\ T^E(\theta, 0) = \sum_{m=-\infty}^{\infty} kJ'_m(k\rho)J_m(kR)\cos(m\theta), & R < \rho, \end{cases} \tag{12}$$

$$L(s, x) = \begin{cases} L^I(\theta, 0) = \sum_{m=-\infty}^{\infty} kJ_m(kR)J'_m(k\rho)\cos(m\theta), & R > \rho, \\ L^E(\theta, 0) = \sum_{m=-\infty}^{\infty} kJ_m(k\rho)J'_m(kR)\cos(m\theta), & R < \rho, \end{cases} \tag{13}$$

$$M(s, x) = \begin{cases} M^I(\theta, 0) = \sum_{m=-\infty}^{\infty} k^2 J'_m(kR)J'_m(k\rho)\cos(m\theta), & R > \rho, \\ M^E(\theta, 0) = \sum_{m=-\infty}^{\infty} k^2 J'_m(k\rho)J'_m(kR)\cos(m\theta), & R < \rho, \end{cases} \tag{14}$$

where the superscripts “ I ” and “ E ” denote the interior and exterior domains, $x = (\rho, 0)$ and $s = (R, \theta)$ in polar coordinate. By superimposing $2N$ lumped density along the boundary, we have the four influence matrices

$$[U_{ij}] = \begin{bmatrix} a_{1,1} & a_{1,2} & a_{1,3} & \cdots & a_{1,2N-1} & a_{1,2N} \\ a_{2,1} & a_{2,2} & a_{2,3} & \cdots & a_{2,2N-1} & a_{2,2N} \\ a_{3,1} & a_{3,2} & a_{3,3} & \cdots & a_{3,2N-1} & a_{3,2N} \\ \vdots & \vdots & \vdots & \ddots & \vdots & \vdots \\ a_{2N,1} & a_{2N,2} & a_{2N,3} & \cdots & a_{2N,2N-1} & a_{2N,2N} \end{bmatrix}, \tag{15}$$

$$[T_{ij}] = \begin{bmatrix} b_{1,1} & b_{1,2} & b_{1,3} & \cdots & b_{1,2N-1} & b_{1,2N} \\ b_{2,1} & b_{2,2} & b_{2,3} & \cdots & b_{2,2N-1} & b_{2,2N} \\ b_{3,1} & b_{3,2} & b_{3,3} & \cdots & b_{3,2N-1} & b_{3,2N} \\ \vdots & \vdots & \vdots & \ddots & \vdots & \vdots \\ b_{2N,1} & b_{2N,2} & b_{2N,3} & \cdots & b_{2N,2N-1} & b_{2N,2N} \end{bmatrix}, \tag{16}$$

$$[L_{ij}] = \begin{bmatrix} c_{1,1} & c_{1,2} & c_{1,3} & \cdots & c_{1,2N-1} & c_{1,2N} \\ c_{2,1} & c_{2,2} & c_{2,3} & \cdots & c_{2,2N-1} & c_{2,2N} \\ c_{3,1} & c_{3,2} & c_{3,3} & \cdots & c_{3,2N-1} & c_{3,2N} \\ \vdots & \vdots & \vdots & \ddots & \vdots & \vdots \\ c_{2N,1} & c_{2N,2} & c_{2N,3} & \cdots & c_{2N,2N-1} & c_{2N,2N} \end{bmatrix}, \tag{17}$$

$$[M_{ij}] = \begin{bmatrix} d_{1,1} & d_{1,2} & d_{1,3} & \cdots & d_{1,2N-1} & d_{1,2N} \\ d_{2,1} & d_{2,2} & d_{2,3} & \cdots & d_{2,2N-1} & d_{2,2N} \\ d_{3,1} & d_{3,2} & d_{3,3} & \cdots & d_{3,2N-1} & d_{3,2N} \\ \vdots & \vdots & \vdots & \ddots & \vdots & \vdots \\ d_{2N,1} & d_{2N,2} & d_{2N,3} & \cdots & d_{2N,2N-1} & d_{2N,2N} \end{bmatrix}, \tag{18}$$

where the elements can be obtained by

$$a_{i,j} = U(s_j, x_i), \quad b_{i,j} = T(s_j, x_i), \tag{19, 20}$$

$$c_{i,j} = L(s_j, x_i), \quad d_{i,j} = M(s_j, x_i). \tag{21, 22}$$

Then, we can determine $\{\phi_j\}$ and $\{\psi_j\}$ by satisfying the boundary conditions.

3. CALCULATION FOR THE DIAGONAL ELEMENTS IN THE FOUR INFLUENCE MATRICES USING THE L'HÔPITAL'S RULE AND INVARIANT METHOD

The diagonal elements in the influence matrices where the radial distance is zero ($r = 0$ when $i = j$) can be solved by using the L'Hôpital's rule. Considering the asymptotic behavior and the recurrence relations of Bessel functions, we can obtain the diagonal elements as follows:

$$\lim_{s \rightarrow x} U(s, x) = \lim_{r \rightarrow 0} J_0(kr) = 1, \tag{23}$$

$$\begin{aligned} \lim_{s \rightarrow x} T(s, x) &= \lim_{r \rightarrow 0} -k \frac{J_1(kr)y_i n_i}{r} \\ &= \lim_{\substack{s_1 \rightarrow x_1 \\ s_2 \rightarrow x_2}} -k^2 \frac{(J_0(kr) - J_2(kr))y_i n_i}{2} = 0, \end{aligned} \tag{24}$$

$$\begin{aligned} \lim_{s \rightarrow x} L(s, x) &= \lim_{r \rightarrow 0} k \frac{J_1(kr)y_j \bar{n}_j}{r} \\ &= \lim_{\substack{s_1 \rightarrow x_1 \\ s_2 \rightarrow x_2}} k^2 \frac{(J_0(kr) - J_2(kr))y_j \bar{n}_j}{2} = 0, \end{aligned} \tag{25}$$

$$\begin{aligned} \lim_{s \rightarrow x} M(s, x) &= \lim_{r \rightarrow 0} k \left(\frac{-kJ_2(kr)y_i y_j n_i \bar{n}_j}{r^2} + \frac{J_1(kr)n_i \bar{n}_i}{r} \right) \\ &= \lim_{\substack{s_1 \rightarrow x_1 \\ s_2 \rightarrow x_2}} 0 + k^2 \frac{(J_0(kr) - J_2(kr))n_i \bar{n}_i}{2} = \frac{k^2}{2}, \end{aligned} \tag{26}$$

where $r = \sqrt{(s_1 - x_1)^2 + (s_2 - x_2)^2}$.

For a circular case, the eigenvalues for the influence matrices in equations (15)–(18) can be obtained by

$$\begin{aligned} \lambda_\ell &= \frac{1}{\rho \Delta \theta} \int_{-\pi}^{\pi} \cos(\ell\theta) \sum_{m=-\infty}^{\infty} J_m(kR)J_m(k\rho)\cos(m\theta)\rho \, d\theta \\ &= 2N J_\ell(k\rho)J_\ell(k\rho), \quad \ell = 0, \pm 1, \dots, \pm(N-1), N, \end{aligned} \tag{27}$$

$$\begin{aligned} \mu_\ell &= \frac{1}{\rho \Delta \theta} \int_{-\pi}^{\pi} \cos(\ell\theta) \sum_{m=-\infty}^{\infty} J'_m(kR)J_m(k\rho)\cos(m\theta)\rho \, d\theta \\ &= 2N(k)J'_\ell(k\rho)J_\ell(k\rho), \quad \ell = 0, \pm 1, \dots, \pm(N-1), N, \end{aligned} \tag{28}$$

$$\begin{aligned} \nu_\ell &= \frac{1}{\rho \Delta \theta} \int_{-\pi}^{\pi} \cos(\ell\theta) \sum_{m=-\infty}^{\infty} J_m(kR)J'_m(k\rho)\cos(m\theta)\rho \, d\theta \\ &= 2N(k)J_\ell(k\rho)J'_\ell(k\rho), \quad \ell = 0, \pm 1, \dots, \pm(N-1), N, \end{aligned} \tag{29}$$

$$\begin{aligned} \kappa_\ell &= \frac{1}{\rho \Delta \theta} \int_{-\pi}^{\pi} \cos(\ell\theta) \sum_{m=-\infty}^{\infty} J'_m(kR)J'_m(k\rho)\cos(m\theta)\rho \, d\theta \\ &= 2N(k^2)J'_\ell(k\rho)J'_\ell(k\rho), \quad \ell = 0, \pm 1, \dots, \pm(N-1), N, \end{aligned} \tag{30}$$

where $\Delta\theta = 2\pi/2N$. According to the addition theorem for the Bessel function and putting the same position for the two points, we have

$$1 = J_0^2(k\rho) + 2 \sum_{m=1}^{\infty} J_m^2(k\rho). \tag{31}$$

By taking derivative with respect to ρ , we have

$$0 = J_0(k\rho)J'_0(k\rho) + 2 \sum_{m=1}^{\infty} J_m(k\rho)J'_m(k\rho). \tag{32}$$

Using the invariant property for the influence matrices, the first invariant is the sum of all the eigenvalues

$$\begin{aligned} 2Na_0 &= \lambda_{-(N-1)} + \dots + \lambda_{-1} + \lambda_0 + \lambda_1 + \dots + \lambda_N \\ &= 2N \sum_{\ell=-\infty}^{\infty} J_\ell(k\rho)J_\ell(k\rho), \end{aligned} \tag{33}$$

$$\begin{aligned} 2Nb_0 &= \mu_{-(N-1)} + \dots + \mu_{-1} + \mu_0 + \mu_1 + \dots + \mu_N \\ &= 2Nk \sum_{\ell=-\infty}^{\infty} J'_\ell(k\rho)J_\ell(k\rho), \end{aligned} \tag{34}$$

$$\begin{aligned}
 2Nc_0 &= v_{-(N-1)} + \dots + v_{-1} + v_0 + v_1 + \dots + v_N \\
 &= 2Nk \sum_{\ell=-\infty}^{\infty} J_\ell(k\rho)J'_\ell(k\rho),
 \end{aligned}
 \tag{35}$$

$$\begin{aligned}
 2Nd_0 &= \kappa_{-(N-1)} + \dots + \kappa_{-1} + \kappa_0 + \kappa_1 + \dots + \kappa_N \\
 &= 2Nk^2 \sum_{\ell=-\infty}^{\infty} J'_\ell(k\rho)J'_\ell(k\rho).
 \end{aligned}
 \tag{36}$$

By substituting equations (31) and (32) into equations (33)–(36), we obtain $a_0 = 1$, $b_0 = 0$, $c_0 = 0$, and $d_0 = k^2/2$ if the imaginary-part kernel was considered. Hence, the indeterminate forms of diagonal elements are easily determined from the first invariant as well as the values obtained by using the L'Hôpital's rule.

4. THE RELATIONS OF KERNELS AND MATRICES BETWEEN THE DIRECT AND INDIRECT METHODS

In solving the boundary-value problem using BEM, two methods, direct method and indirect method are employed. The direct method is derived by using the Green identity in terms of the unknowns which are the actual physical quantities on the boundary. In the direct method, we have

$$0 = \int_B T^E(s, x)u(s) \, dB(s) - \int_B U^E(s, x)t(s) \, dB(s),
 \tag{37}$$

$$0 = \int_B M^E(s, x)u(s) \, dB(s) - \int_B L^E(s, x)t(s) \, dB(s),
 \tag{38}$$

where $u(s)$ and $t(s)$ are the potential and its normal derivative on the boundary and x is outside the domain.

A key point of the indirect method is to represent a solution which satisfies the governing equation. The unknown densities are determined by matching the boundary conditions. Based on the superposition principle for the potentials, we have

Single-layer potential approach:

$$u(x) = \int_B U^I(s, x)\phi(s) \, dB(s),
 \tag{39}$$

$$t(x) = \int_B L^I(s, x)\phi(s) \, dB(s).
 \tag{40}$$

Double-layer potential approach:

$$u(x) = \int_B T^I(s, x)\psi(s) \, dB(s),
 \tag{41}$$

$$t(x) = \int_B M^I(s, x)\psi(s) \, dB(s),
 \tag{42}$$

where $\phi(s)$ and $\psi(s)$ are the single- and double-layer unknown densities, respectively. By discretizing equations (37) and (38), we have the linear algebraic equations for the direct method

$$[T^E_{ij}]\{u_j\} = [U^E_{ij}]\{t_j\},
 \tag{43}$$

TABLE 1

The distributed and concentrated-type of imaginary-part method for the single- and double-layer potential approaches

	Distributed-type	Concentrated-type [†]
Single-layer potential approach	Dirichlet problem: $u(x) = \int_B U^I(s, x)\phi(s) \, dB(s)$ Neumann problem: $t(x) = \int_B L^I(s, x)\phi(s) \, dB(s)$	Dirichlet problem: $u(x_i) = \sum_j U^I(s_j, x_i)A_j = (SM)_{ij}A_j$ Neumann problem: $t(x_i) = \sum_j L^I(s_j, x_i)A_j = (SM_x)_{ij}A_j$
Double-layer potential approach	Dirichlet problem: $u(x) = \int_B T^I(s, x)\psi(s) \, dB(s)$ Neumann problem: $t(x) = \int_B M^I(s, x)\psi(s) \, dB(s)$	Dirichlet problem: $u(x_i) = \sum_j T^I(s_j, x_i)B_j = (SM_s)_{ij}B_j$ Neumann problem: $t(x_i) = \sum_j M^I(s_j, x_i)B_j = (SM_{sx})_{ij}B_j$

[†] NDIF method by Kang *et al.* [14–16] is the special case.

$$[M_{ij}^E]\{u_j\} = [L_{ij}^E]\{t_j\}, \tag{44}$$

where $\{u_j\}$ and $\{t_j\}$ are the potential and its normal derivative on the boundary B . By discretizing equations (39)–(42), we have the linear algebraic equations for the indirect method.

Single-layer potential approach:

$$u(x_i) = [U_{ij}^I]\{\phi_j\}, \tag{45}$$

$$t(x_i) = [L_{ij}^I]\{\phi_j\}. \tag{46}$$

Double-layer potential approach:

$$u(x_i) = [T_{ij}^I]\{\psi_j\}, \tag{47}$$

$$t(x_i) = [M_{ij}^I]\{\psi_j\}, \tag{48}$$

where $\{\phi_j\}$ and $\{\psi_j\}$ are the single- and double-layer unknown densities, respectively. The distributed-type and concentrated-type of imaginary-part method for the single- and double-layer potential approaches are shown in Table 1. By considering the degenerate kernels equations (11)–(14) and comparing with equations (43)–(48), we can find the following relations between the interior and exterior kernels from equations (11)–(14), i.e.,

$$U_{ij}^E = U_{ij}^I \text{ or } U^E(s, x) = U^I(x, s), \tag{49}$$

$$T_{ij}^E = L_{ij}^I \text{ or } T^E(s, x) = L^I(x, s), \tag{50}$$

$$L_{ij}^E = T_{ij}^I \text{ or } L^E(s, x) = T^I(x, s), \tag{51}$$

$$M_{ij}^E = M_{ij}^I \text{ or } M^E(s, x) = M^I(x, s). \tag{52}$$

TABLE 2

SVD updating technique for the true and spurious eigensolutions for a circular cavity using the direct and indirect methods

Boundary-value problem	Eigensolutions	Density function		True and spurious eigenvalues			
		Single-layer potential approach	Double-layer potential approach	Direct method		Indirect method	
Dirichlet problem	True eigensolution	$J_m(k\rho) = 0$ (Figure 1(a))	$J_m(k\rho) = 0$ (Figure 1(b))	SVD updating term	$\begin{bmatrix} U^E \\ L^E \end{bmatrix}$	SVD updating term	$\begin{bmatrix} U^I \\ T^I \end{bmatrix}$ (Figure 1(c))
	Spurious eigensolution	$J_m(k\rho) = 0$ (Figure 1(a))	$J'_m(k\rho) = 0$ (Figure 1(b))	SVD updating document	$\begin{bmatrix} L^E & M^E \end{bmatrix}$	SVD updating document	$\begin{bmatrix} T^I & M^I \end{bmatrix}$ (Figure 1(d))
Neumann problem	True eigensolution	$J'_m(k\rho) = 0$ (Figure 2(a))	$J'_m(k\rho) = 0$ (Figure 2(b))	SVD updating term	$\begin{bmatrix} T^E \\ M^E \end{bmatrix}$	SVD updating term	$\begin{bmatrix} L^I \\ M^I \end{bmatrix}$ (Figure 2(c))
	Spurious eigensolution	$J_m(k\rho) = 0$ (Figure 2(a))	$J'_m(k\rho) = 0$ (Figure 2(b))	SVD updating document	$\begin{bmatrix} U^E & T^E \end{bmatrix}$	SVD updating document	$\begin{bmatrix} U^I & L^I \end{bmatrix}$ (Figure 2(d))

Note: $U^I = U^E$, $L^I = T^E$, $T^I = L^E$ and $M^I = M^E$.

5. DERIVATION OF TRUE AND SPURIOUS EIGENSOLUTIONS FOR THE CIRCULAR CAVITY USING THE DEGENERATE KERNELS

In the circular cavity, we have the degenerate kernel functions in equations (11)–(14). We assume the single- and double-layer density functions on the boundary as

$$\phi(s) = \sum_{n=-\infty}^{\infty} (A_n \cos(n\theta) + B_n \sin(n\theta)), \tag{53}$$

$$\psi(s) = \sum_{n=-\infty}^{\infty} (C_n \cos(n\theta) + D_n \sin(n\theta)), \tag{54}$$

where A_n, B_n, C_n and D_n are coefficients. For the Dirichlet problem, equation (39) reduced to

$$\begin{aligned} 0 &= \int_B U^I(s, x)\phi(s) dB(s) \\ &= \int_0^{2\pi} \sum_{m=-\infty}^{\infty} J_m(kR)J_m(k\rho) \cos(m\theta) \sum_{n=-\infty}^{\infty} (A_n \cos(n\theta) + B_n \sin(n\theta)) \rho d\theta, \end{aligned} \tag{55}$$

by using equation (53). By considering the orthogonality of trigonometric function, we have

$$\int_0^{2\pi} \cos(m\theta) \cos(n\theta) d\theta = \begin{cases} \pi, & m = n, \\ 0, & m \neq n, \end{cases} \tag{56}$$

$$\int_0^{2\pi} \cos(m\theta) \sin(n\theta) d\theta = 0. \tag{57}$$

According to equation (56) and equation (57), equation (55) simplifies to

$$\begin{aligned} 0 &= \int_0^{2\pi} \sum_{m=-\infty}^{\infty} J_m(kR)J_m(k\rho)\cos(m\theta) \sum_{n=-\infty}^{\infty} (A_n \cos(n\theta) + B_n \sin(n\theta)) \rho d\theta, \\ &= \pi \sum_{m=-\infty}^{\infty} A_m J_m(kR)J_m(k\rho). \end{aligned} \tag{58}$$

TABLE 3

Zeros of the Bessel functions and its derivative, $J_n(k)$ and $J'_n(k)$

Problem	Eigenvalues	1	2	3	4	5
Dirichlet problem	$J_0(k)$	2.4042	5.5201	8.6537	11.7915	14.9309
	$J_1(k)$	3.8317	7.0156	10.1735	13.3237	16.4706
	$J_2(k)$	5.1356	8.4172	11.6198	14.7959	17.9598
	$J_n(k)$	6.3802	9.7610	13.0152	16.2234	19.4094
	$J_4(k)$	7.5883	11.0647	14.3725	17.6160	20.8269
	$J_5(k)$	8.7715	12.3386	15.7002	18.9801	22.2178
Neumann problem	$J'_0(k)$	0	3.8317	7.0156	10.1735	13.3237
	$J'_1(k)$	1.8412	5.3314	8.5363	11.7060	14.8636
	$J'_2(k)$	3.0542	6.7071	9.9695	13.1703	16.3475
	$J'_3(k)$	4.2012	8.0152	11.3459	14.5858	17.7887
	$J'_4(k)$	5.3175	9.2824	12.6819	15.9641	19.1960
	$J'_5(k)$	6.4156	10.5199	13.9872	17.3128	20.5755

Thus, we obtain the eigenequation $J_m(kR)J_m(k\rho) = 0$ by using the single-layer potential methods for the interior Dirichlet problem.

Similarly, we also obtain

$$\begin{aligned}
 0 &= \int_B T^I(s, x)\psi(s) dB(s) \\
 &= \int_0^{2\pi} \sum_{m=-\infty}^{\infty} kJ'_m(kR)J_m(k\rho)\cos(m\theta) \sum_{n=-\infty}^{\infty} (C_n \cos(n\theta) + D_n \sin(n\theta)) \rho d\theta \quad (59)
 \end{aligned}$$

by using the double-layer potential approach. By considering equation (59) and the orthogonality of trigonometric function, we have

$$\begin{aligned}
 0 &= \int_0^{2\pi} \sum_{m=-\infty}^{\infty} kJ'_m(kR)J_m(k\rho)\cos(m\theta) \sum_{n=-\infty}^{\infty} (C_n \cos(n\theta) + D_n \sin(n\theta)) \rho d\theta \\
 &= \pi k \sum_{m=-\infty}^{\infty} C_m J'_m(kR)J_m(k\rho). \quad (60)
 \end{aligned}$$

Thus, we obtain the eigenequation $J'_m(kR)J_m(k\rho) = 0$ by using the double-layer potential method for the interior Dirichlet problem.

In the Neumann problem, we have

$$\begin{aligned}
 0 &= \int_B L^I(s, x)\phi(s) dB(s) \\
 &= \int_0^{2\pi} \sum_{m=-\infty}^{\infty} kJ_m(kR)J'_m(k\rho)\cos(m\theta) \sum_{n=-\infty}^{\infty} (A_n \cos(n\theta) + B_n \sin(n\theta)) \rho d\theta \quad (61)
 \end{aligned}$$

by substituting equations (13) and (53) into equation (40). By considering the orthogonality of trigonometric function, equation (61) simplifies to

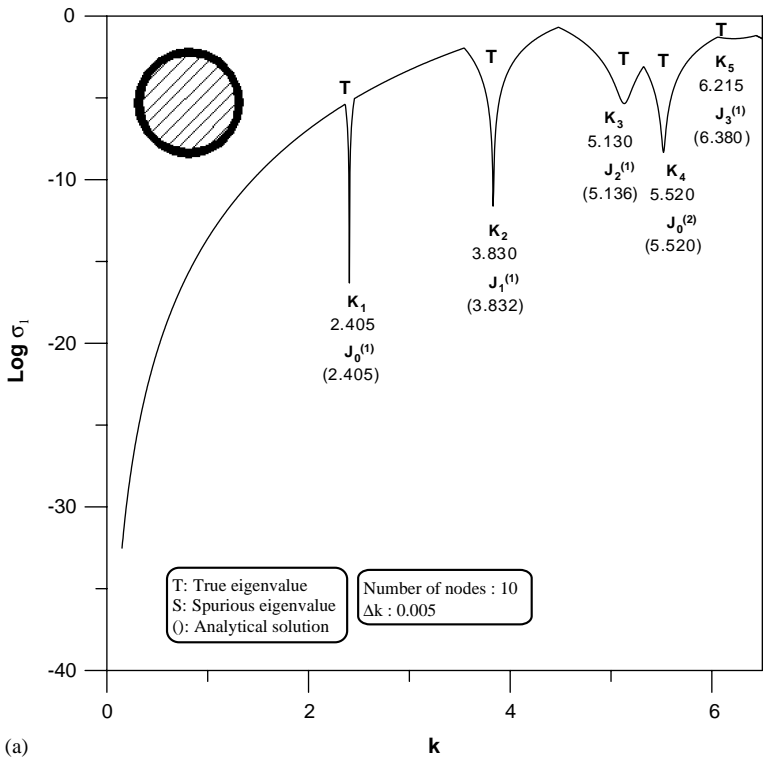
$$\begin{aligned}
 0 &= \int_0^{2\pi} \sum_{m=-\infty}^{\infty} kJ_m(kR)J'_m(k\rho)\cos(m\theta) \sum_{n=-\infty}^{\infty} (A_n \cos(n\theta) + B_n \sin(n\theta)) \rho d\theta \\
 &= \pi k \sum_{m=-\infty}^{\infty} A_m J_m(kR)J'_m(k\rho). \quad (62)
 \end{aligned}$$

Therefore, we obtain the eigenequation $J_m(kR)J'_m(k\rho) = 0$ by using the single-layer potential method for the interior Neumann problem.

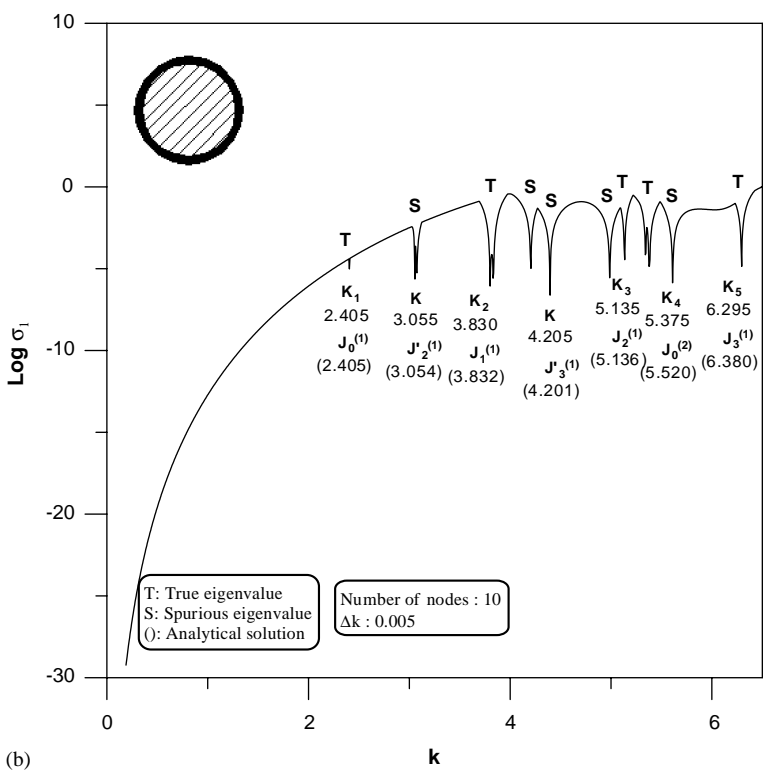
Similarly, we use the double-layer density functions to obtain

$$\begin{aligned}
 0 &= \int_B M^I(s, x)\psi(s) dB(s) \\
 &= \int_0^{2\pi} \sum_{m=-\infty}^{\infty} k^2 J'_m(kR)J'_m(k\rho)\cos(m\theta) \sum_{n=-\infty}^{\infty} (C_n \cos(n\theta) + D_n \sin(n\theta)) \rho d\theta. \quad (63)
 \end{aligned}$$

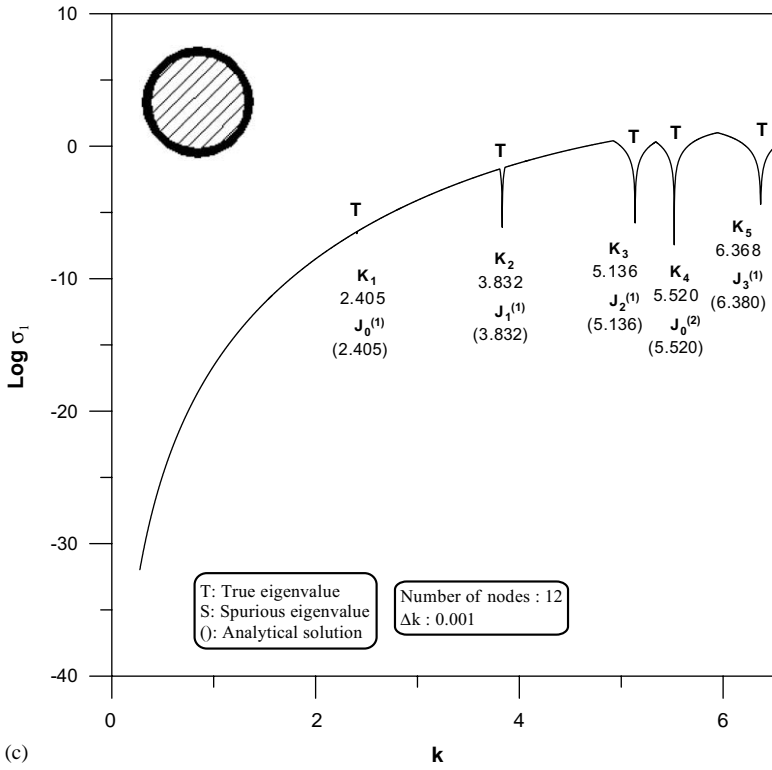
Figure 1. (a) The minimum singular value for different wave numbers by using the single-layer potential approach for the Dirichlet problem. (b) The minimum singular value for different wave numbers by using the double-layer potential approach for the Dirichlet problem. (c) The minimum singular value for different wave numbers using the SVD updating term $[U \ T]$ for the Dirichlet problem. (d) The minimum singular value for different wave numbers using the SVD updating document $[T \ M]$ for the Dirichlet problem. (e) The former three interior modes by using the single-layer potential approach for the Dirichlet problem. (f) The former three interior modes matrix by using the double-layer potential approach for the Dirichlet problem. (g) The former three analytical interior modes for the Dirichlet problem.



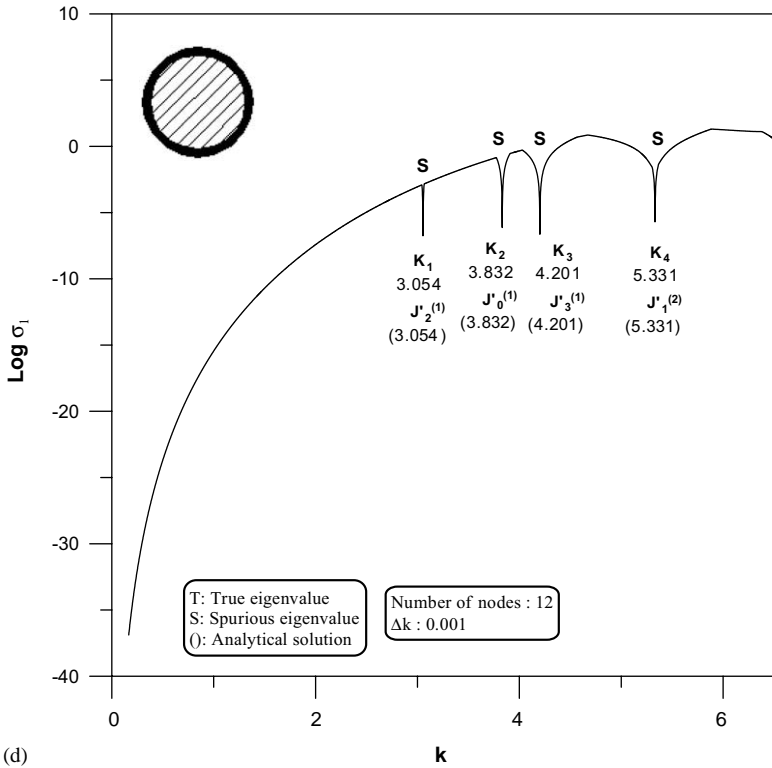
(a)



(b)

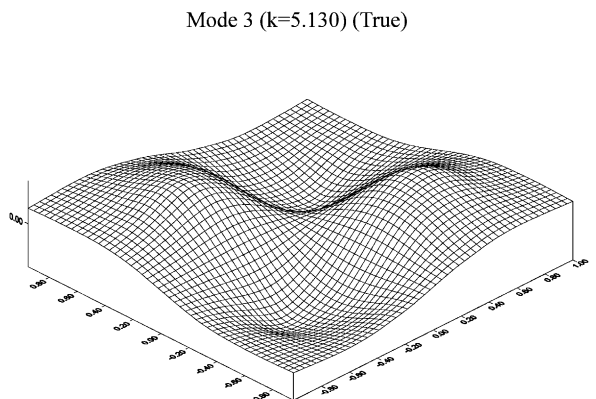
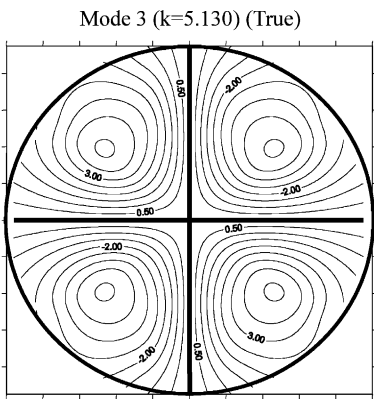
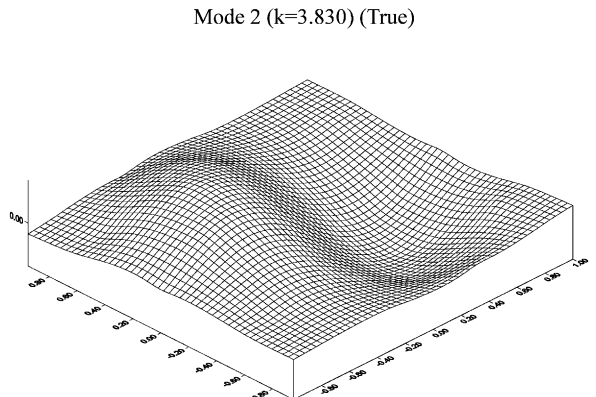
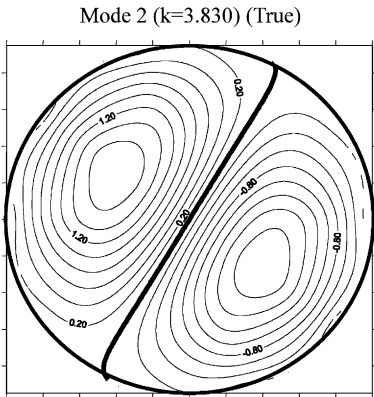
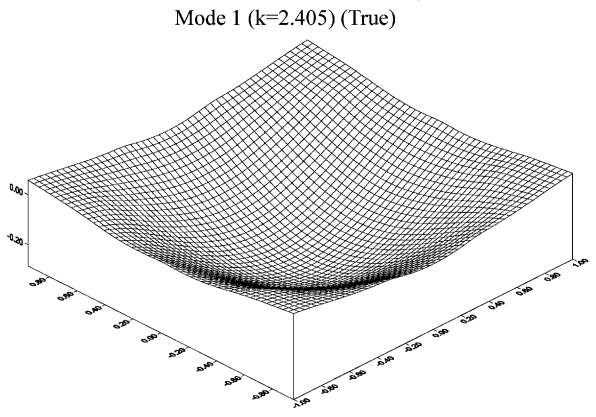
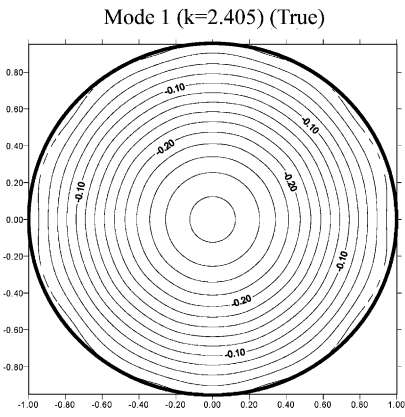


(c)



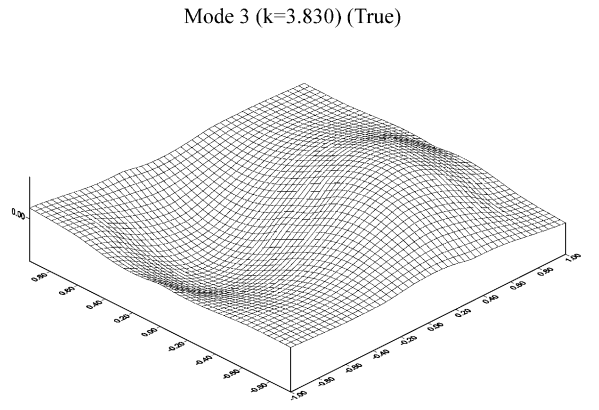
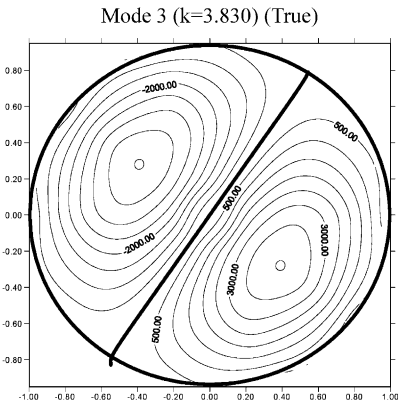
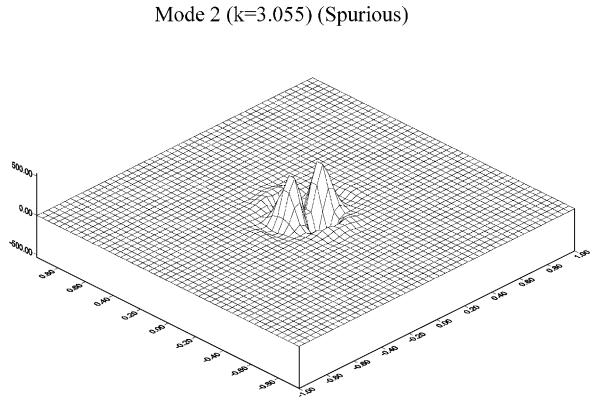
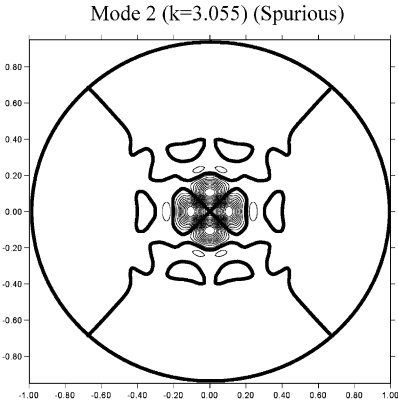
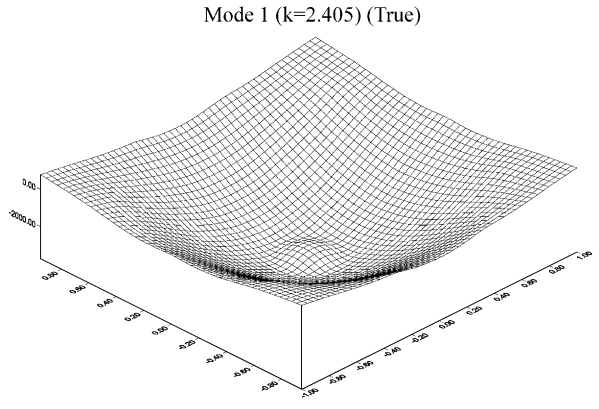
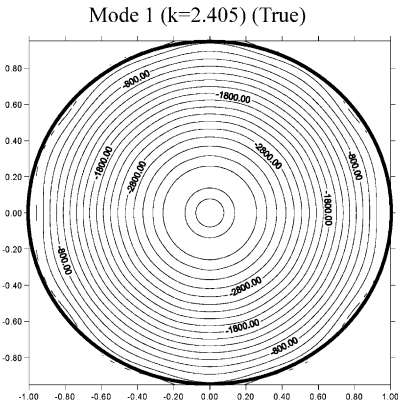
(d)

Figure 1. Continued.



(e)

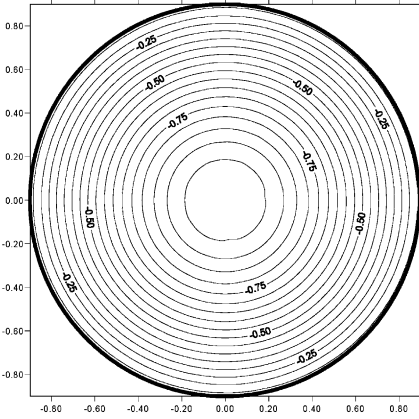
Figure 1. Continued.



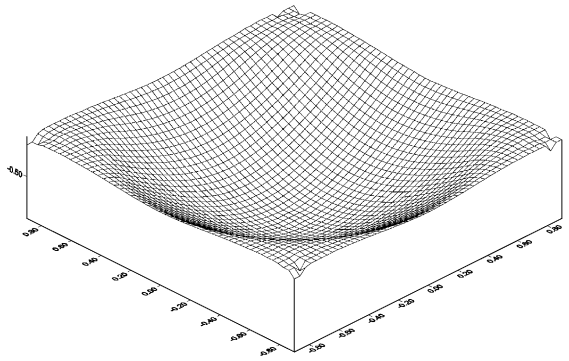
(f)

Figure 1. Continued.

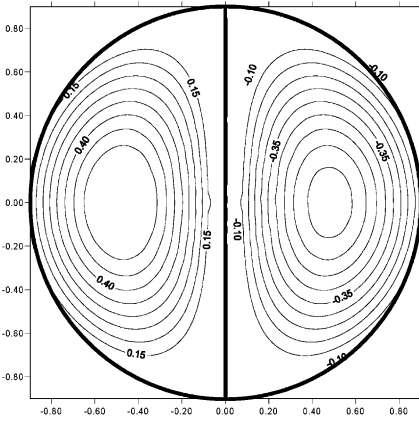
Mode 1 ($k=2.404$)



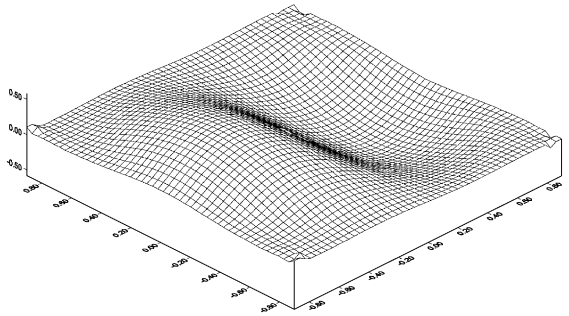
Mode 1 ($k=2.404$)



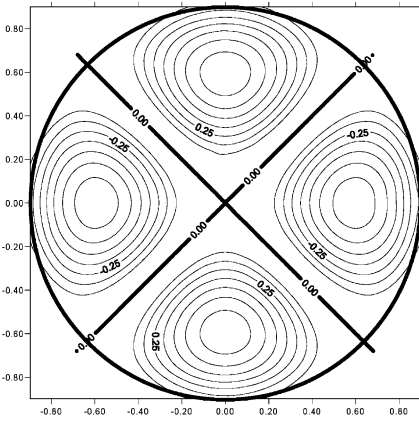
Mode 2 ($k=3.832$)



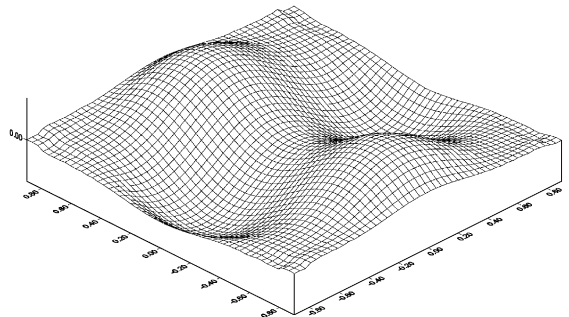
Mode 2 ($k=3.832$)



Mode 3 ($k=5.136$)



Mode 3 ($k=5.136$)



(g)

Figure 1. Continued.

By considering equation (63) and the orthogonality of trigonometric function, we have

$$\begin{aligned}
 0 &= \int_0^{2\pi} \sum_{m=-\infty}^{\infty} k^2 J'_m(kR) J'_m(k\rho) \cos(m\theta) \sum_{n=-\infty}^{\infty} (C_n \cos(n\theta) + D_n \sin(n\theta)) \rho \, d\theta \\
 &= \pi k^2 \sum_{m=-\infty}^{\infty} C_m J'_m(kR) J'_m(k\rho).
 \end{aligned}
 \tag{64}$$

Therefore, we obtain the eigenequation $J'_n(kR)J'_n(k\rho) = 0$ by using the double-layer potential method for the interior Neumann problem. All the relations of true and spurious eigenvalues by using the single- and double-layer potential approaches are summarized in Table 2.

6. METHOD TO EXTRACT OUT THE TRUE EIGENSOLUTIONS

The SVD technique is an important tool in linear algebra. A matrix A with dimension $M \times N$ can be decomposed into a product of an orthogonal matrix Ψ ($N \times N$), a diagonal matrix Σ ($M \times N$) with positive or zero elements, and an orthogonal matrix Φ ($M \times M$),

$$[A]_{M \times N} = [\Phi]_{M \times M} [\Sigma]_{M \times N} [\Psi]_{N \times N}^T,
 \tag{65}$$

where the superscript ‘‘T’’ is the transpose, Φ and Ψ are both orthogonal in the sense that their column vectors are orthogonal,

$$\phi_i \cdot \phi_j = \delta_{ij},
 \tag{66}$$

$$\psi_i \cdot \psi_j = \delta_{ij},
 \tag{67}$$

where $\Phi^T \Phi = \Psi^T \Psi = I$ and δ_{ij} is the Kronecker delta symbol. Besides, we solve a homogeneous equation and obtain a non-trivial solution from a column vector $\{\psi_i\}$ of Ψ such that the singular value (σ_i) is zero. For the direct method in the discrete system, equations (43) and (44) are represented by

Singular equation:

$$(\text{UT method}) \quad [T^E]\{u\} = [U^E]\{t\} = 0,
 \tag{68}$$

Hypersingular equation:

$$(\text{LM method}) \quad [M^E]\{u\} = [L^E]\{t\} = 0.
 \tag{69}$$

TABLE 4

True and spurious eigensolutions for the Dirichlet and Neumann problems using the present formulation

Indirect formulation	Dirichlet problem	Neumann problem
Single-layer potential approach		
True mode	$-\pi J_n(ka) J_n(k\rho) \cos(n\phi)^\dagger$	$-\pi k J'_n(ka) J_n(k\rho) \cos(n\phi)$
Spurious mode	$-\pi J_n(ka) J_n(k\rho) \cos(n\phi)^\dagger$	$-\pi k J'_n(ka) J_n(k\rho) \cos(n\phi)^\dagger$
Double-layer potential approach		
True mode	$-\pi J_n(ka) J'_n(k\rho) \cos(n\phi)$	$-\pi k^2 J'_n(ka) J'_n(k\rho) \cos(n\phi)^\dagger$
Spurious mode	$-\pi J_n(ka) J'_n(k\rho) \cos(n\phi)^\dagger$	$-\pi k^2 J'_n(ka) J'_n(k\rho) \cos(n\phi)^\dagger$

Note: $0 < a < \rho, 0 < \phi < 2\pi$.

† Denotes a near-zero solution.

For the Dirichlet problem, equations (68) and (69) are combined to

$$\begin{bmatrix} [U^E] \\ [L^E] \end{bmatrix} \{t\} = \{0\}. \tag{70}$$

By using the SVD technique, the two matrices in equation (70) are decomposed into

$$[U^E] = [\Phi^U][\Sigma^U][\Psi^U]^T \quad \text{or} \quad [U_j^E] = \sum_j \sigma_j^U \{\phi_j^U\} \{\psi_j^U\}^T,$$

$$[L^E] = [\Phi^L][\Sigma^L][\Psi^L]^T \quad \text{or} \quad [L_j^E] = \sum_j \sigma_j^L \{\phi_j^L\} \{\psi_j^L\}^T. \tag{71}$$

For the linear algebraic system, t is one column vector $\{\psi_i\}$ in the $[\Psi]$ matrix corresponding to the zero singular value ($\sigma_i = 0$). By viewing t as a $\{\psi_i\}$ vector in the right unitary matrix $[\Psi]$, equation (70) reduces to

$$[U^E] \{\psi_i\} = \{0\},$$

$$[L^E] \{\psi_i\} = \{0\}, \tag{72}$$

since

$$\sum_j \sigma_j^U \{\phi_j^U\} \{\psi_j^U\}^T \{\psi_i\} = \{0\} \quad \xrightarrow{\psi_j^U \cdot \psi_j = \delta_{ij}} \quad \sigma_i^U \{\phi_i^U\} = \{0\} \quad (i \text{ no sum}),$$

$$\sum_j \sigma_j^L \{\phi_j^L\} \{\psi_j^L\}^T \{\psi_i\} = \{0\} \quad \xrightarrow{\psi_j^L \cdot \psi_j = \delta_{ij}} \quad \sigma_i^L \{\phi_i^L\} = \{0\}, \quad (i \text{ no sum}), \tag{73}$$

where $\{\phi_i\}$ and $\{\psi_i\}$ are the orthonormal bases, σ_j^U and σ_j^L are the singular values of $[U^E]$ and $[L^E]$ matrices, respectively. We can easily extract out the true eigensolutions ($\sigma_i^U = \sigma_i^L = 0$) since there exists the same eigensolution ($t = \{\psi_i\}$) in the Dirichlet problem using equations (70)–(73) together. In a similar way, equations (68) and (69) are combined to

$$\begin{bmatrix} [T^E] \\ [M^E] \end{bmatrix} \{u\} = \{0\} \tag{74}$$

for the Neumann problem. We can easily extract the true eigensolutions;

$$\sum_j \sigma_j^T \{\phi_j\} \{\psi_j\}^T \{\psi_i\} = \{0\} \quad \xrightarrow{\psi_i \cdot \psi_j = \delta_{ij}} \quad \sigma_i^T \{\phi_i\} = \{0\} \quad (i \text{ no sum}),$$

$$\sum_j \sigma_j^M \{\phi_j\} \{\psi_j\}^T \{\psi_i\} = \{0\} \quad \xrightarrow{\psi_i \cdot \psi_j = \delta_{ij}} \quad \sigma_i^M \{\phi_i\} = \{0\} \quad (i \text{ no sum}), \tag{75}$$

since there exists the same solution ($u = \{\psi_i\}$) corresponding to the zero singular values ($\sigma_i^T = \sigma_i^M = 0$) by using equations (74) and (75).

According to the relations between the direct method and indirect method (equations (49)–(52)), we can extend to extract out the true solutions in the indirect method. For the Dirichlet problem, equation (70) changes to

$$\begin{bmatrix} [U^E] \\ [L^E] \end{bmatrix} \{t\} = \{0\} \xrightarrow{\substack{U^E=U^I \\ L^E=T^I}} \begin{bmatrix} [U^I] \\ [T^I] \end{bmatrix} \{t\} = \{0\}, \tag{76}$$

after using equations (49)–(51). By using the SVD technique and equation (76), we have

$$\sum_j \sigma_j^U \{\phi_j\} \{\psi_j\}^T \{\psi_i\} = \{0\} \quad \xrightarrow{\psi_i \cdot \psi_j = \delta_{ij}} \quad \sigma_i^U \{\phi_i\} = \{0\} \quad (i \text{ no sum}),$$

$$\sum_j \sigma_j^T \{\phi_j\} \{\psi_j\}^T \{\psi_i\} = \{0\} \xrightarrow{\psi_i, \psi_j = \delta_{ij}} \sigma_i^T \{\phi_i\} = \{0\} \quad (i \text{ no sum}), \tag{77}$$

where $\{\psi_i\}$ is an orthonormal basis; σ_j^U and σ_j^T are the singular values of $[U^I]$ and $[T^I]$ matrices, respectively. We can easily extract the true solutions in the Dirichlet problem by using equation (77) for the zero singular values of $\sigma_i^U = \sigma_i^T = 0$.

In a similar way, equation (74) changes to

$$\begin{bmatrix} [T^E] \\ [M^E] \end{bmatrix} \{t\} = \{0\} \xrightarrow{\frac{T^E=L^I}{M^E=M^I}} \begin{bmatrix} [L^I] \\ [M^I] \end{bmatrix} \{t\} = \{0\}, \tag{78}$$

after using equations (50)–(52). By using the SVD technique and equation (78), we have

$$\begin{aligned} \sum_j \sigma_j^L \{\phi_j\} \{\psi_j\}^T \{\psi_i\} = \{0\} &\xrightarrow{\psi_i, \psi_j = \delta_{ij}} \sigma_i^L \{\phi_i\} = \{0\} \quad (i \text{ no sum}), \\ \sum_j \sigma_j^M \{\phi_j\} \{\psi_j\}^T \{\psi_i\} = \{0\} &\xrightarrow{\psi_i, \psi_j = \delta_{ij}} \sigma_i^M \{\phi_i\} = \{0\} \quad (i \text{ no sum}), \end{aligned} \tag{79}$$

where $\{\psi_i\}$ is an orthonormal basis, σ_j^L and σ_j^M are the singular values of $[L^I]$ and $[M^I]$ matrices, respectively. We can easily extract out the true eigensolutions in the Neumann problem by using equation (79) for the zero singular values of $\sigma_i^L = \sigma_i^M = 0$.

6.1. EXTRACTING OUT THE TRUE EIGENSOLUTIONS BY USING THE SVD UPDATING TERM FOR A CIRCULAR CASE

For a circular cavity subject to the Dirichlet boundary condition, we obtain the two eigenequations

$$\text{Single-layer approach : } J_i(k\rho)J_i(k\rho) = 0 \quad (i \text{ no sum}), \tag{80}$$

$$\text{Double-layer approach : } J_i(k\rho)J_i'(k\rho) = 0 \quad (i \text{ no sum}). \tag{81}$$

The true eigensolution $J_i(k\rho) = 0$ satisfies both equations and the spurious eigensolutions $J_i'(k\rho) = 0$ satisfies only one of the equations by using the double-layer potential approach for the Dirichlet problem.

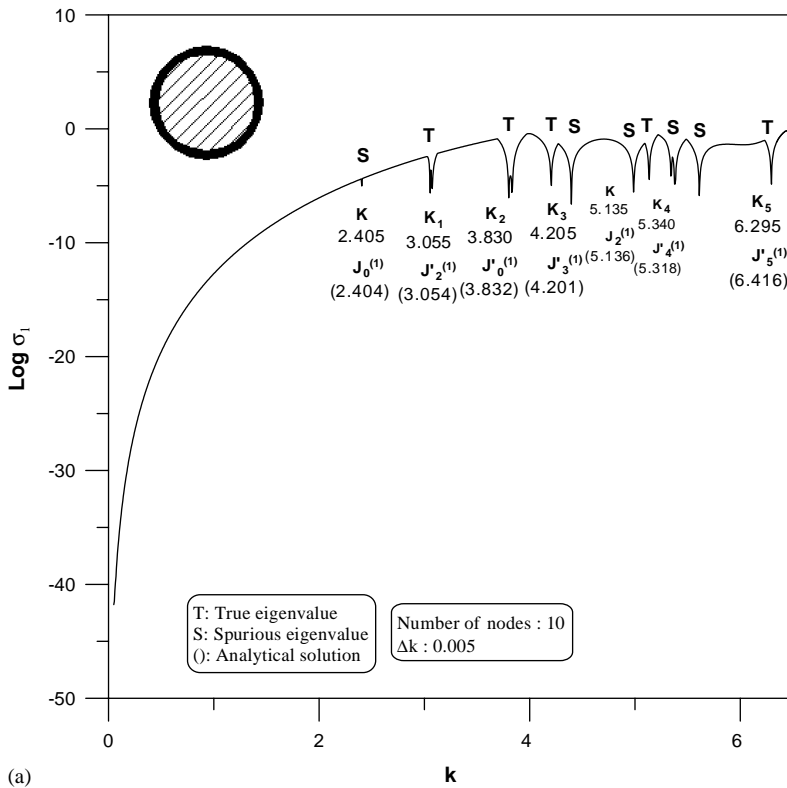
To obtain an overdetermined system for the Dirichlet problem, we can combine $[U^I]$ and $[T^I]$ matrices by using the updating terms,

$$[C] = \begin{bmatrix} [U^I] \\ [T^I] \end{bmatrix}_{4N \times 2N}. \tag{82}$$

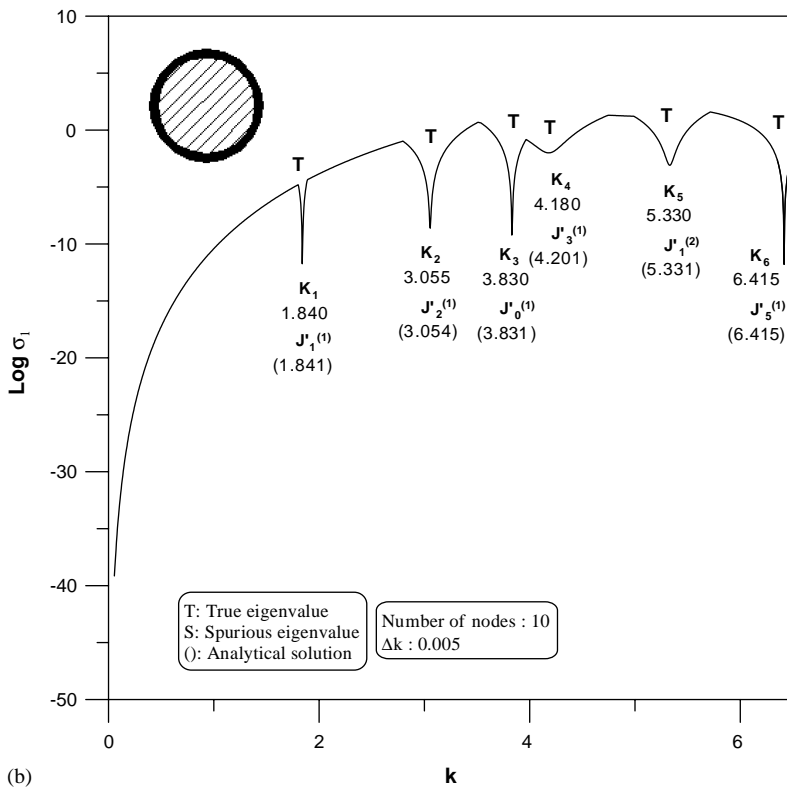
Since the eigensolution is non-trivial, the rank of $[C]$ must be smaller than $2N$. Therefore, the $2N$ singular values for $[C]$ matrix must have at least one zero value. Based on the equivalence between the SVD technique and the least-squares method in the mathematical

➔

Figure 2. (a) The minimum singular value for different wave numbers by using the single-layer potential approach for the Neumann problem. (b) The minimum singular value for different wave numbers by using the double-layer potential approach for the Neumann problem. (c) The minimum singular value for different wave numbers by using the SVD updating term $[L \ M]$ for the Neumann problem. (d) The minimum singular value for different wave numbers by using the SVD updating document $[U \ L]$ for the Neumann problem. (e) The former three interior modes by using the single-layer potential approach for the Neumann problem. (f) The former three interior modes by using the double-layer potential approach for the Neumann problem. (g) The former three analytical interior modes for the Neumann problem.



(a)



(b)

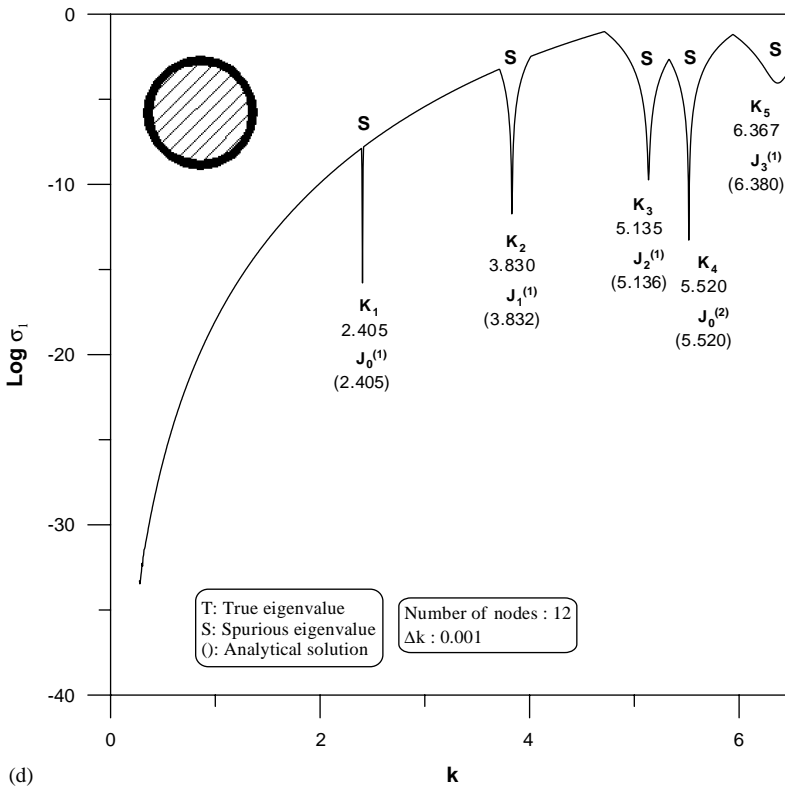
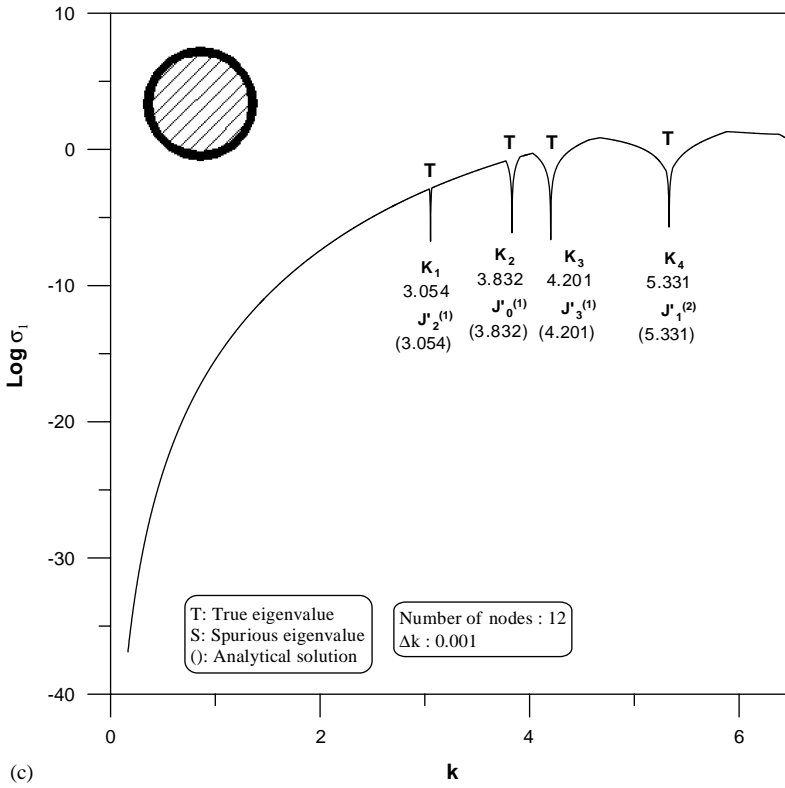
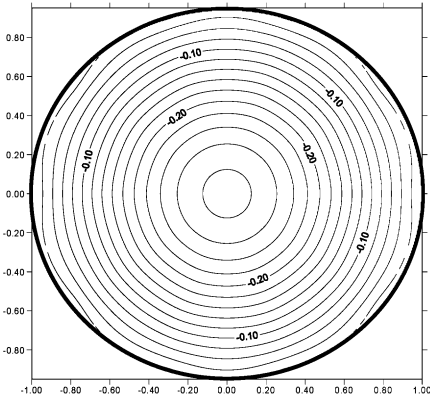
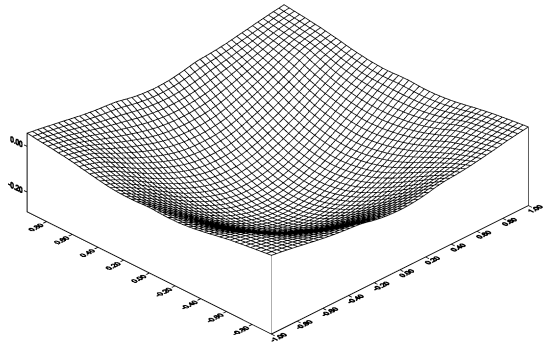


Figure 2. Continued.

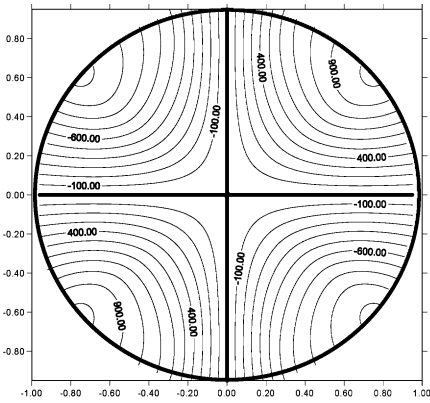
Mode 1 ($k=2.405$) (Spurious)



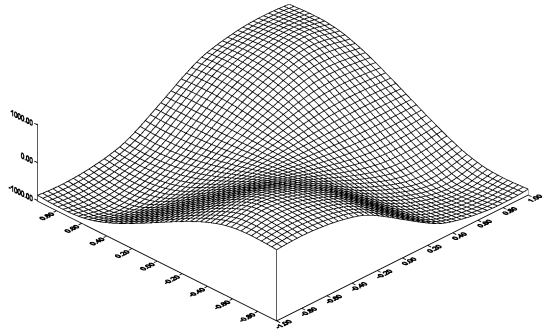
Mode 1 ($k=2.405$) (Spurious)



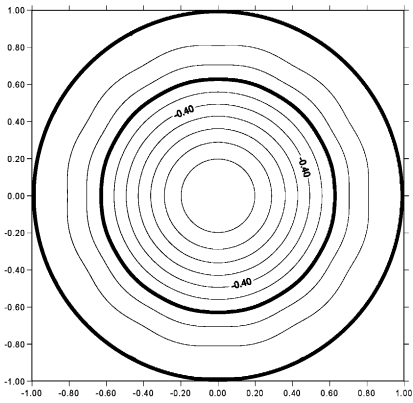
Mode 2 ($k=3.055$) (True)



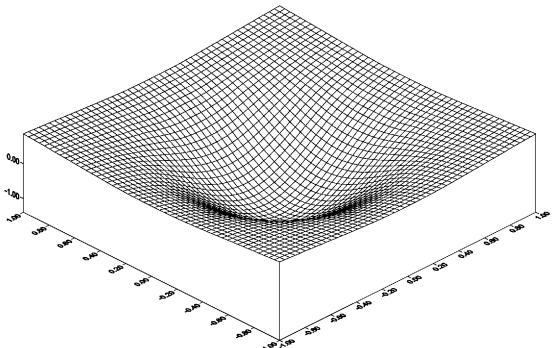
Mode 2 ($k=3.055$) (True)



Mode 3 ($k=3.830$) (True)



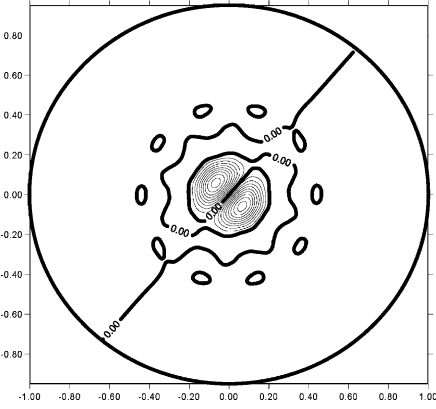
Mode 3 ($k=3.830$) (True)



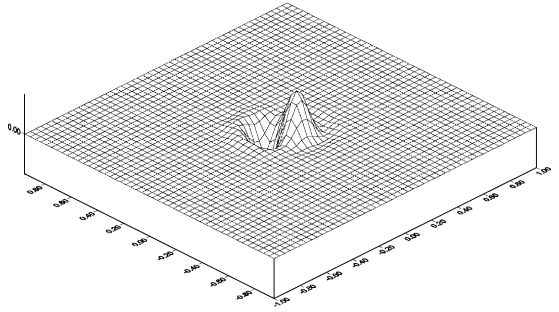
(e)

Figure 2. Continued.

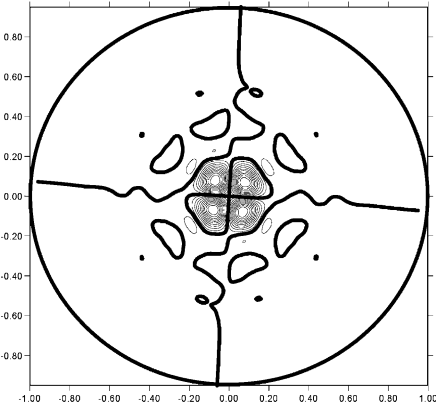
Mode 1 ($k=1.840$) (True)



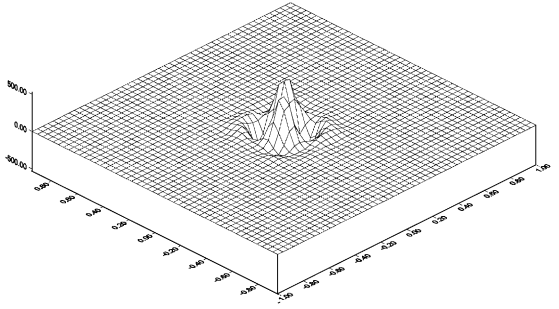
Mode 1 ($k=1.840$) (True)



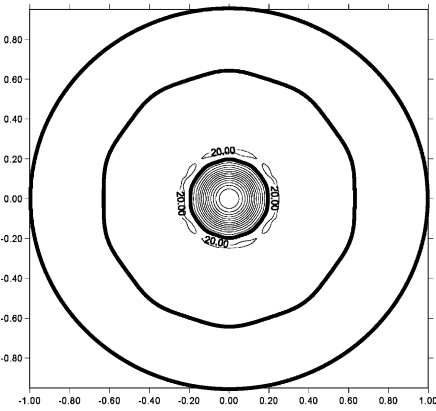
Mode 2 ($k=3.055$) (True)



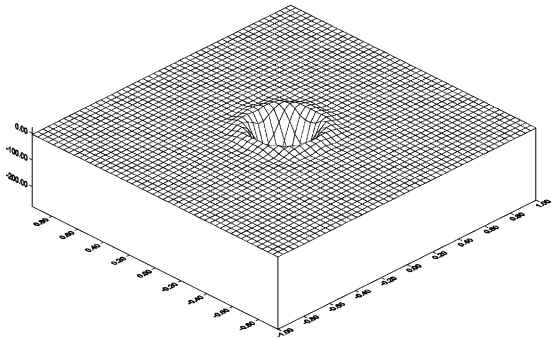
Mode 2 ($k=3.055$) (True)



Mode 3 ($k=3.830$) (True)



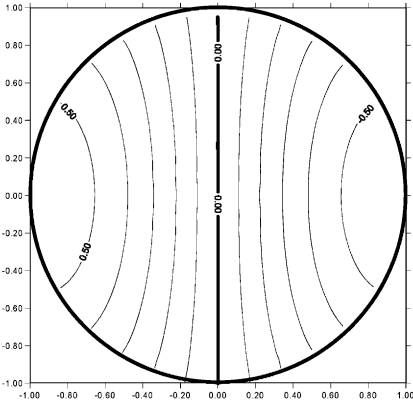
Mode 3 ($k=3.83$) (True)



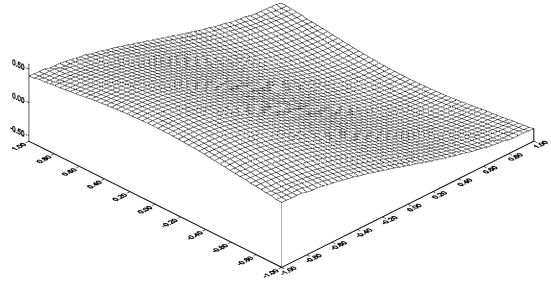
(f)

Figure 2. Continued.

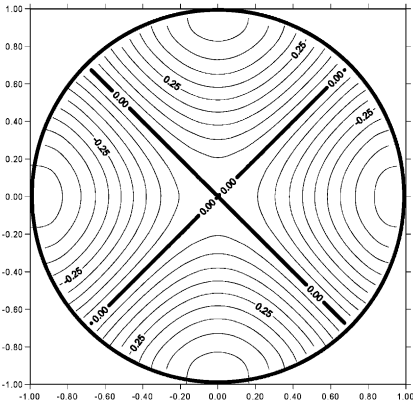
Mode 1 ($k=1.841$)



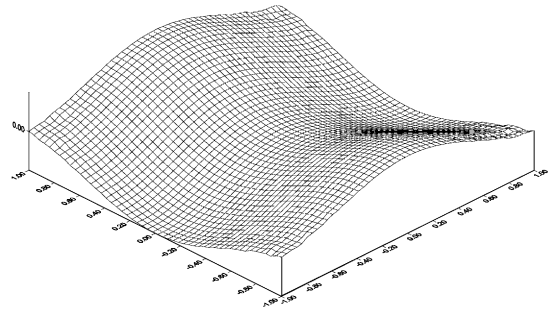
Mode 1 ($k=1.841$)



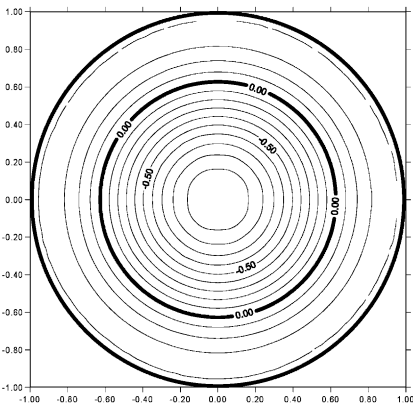
Mode 2 ($k=3.054$)



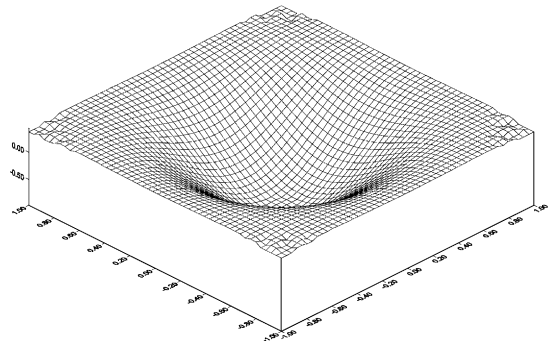
Mode 2 ($k=3.054$)



Mode 3 ($k=3.832$)



Mode 3 ($k=3.832$)



(g)

Figure 2. Continued.

essence, we have

$$\begin{bmatrix} [U^I]^T & [T^I]^T \end{bmatrix} \begin{bmatrix} [U^I] \\ [T^I] \end{bmatrix} = [U^I]^2 + [T^I]^2. \tag{83}$$

For the special case of a circular cavity in the Dirchlet problem, we can decompose $[U^I]$ and $[T^I]$ into

$$[U^I] = [\Phi] \begin{bmatrix} \ddots & & & & \\ & \lambda_\ell & & & \\ & & \ddots & & \\ & & & \ddots & \\ & & & & \ddots \end{bmatrix} [\Phi]^T, \tag{84}$$

$$[T^I] = [\Phi] \begin{bmatrix} \ddots & & & & \\ & \mu_\ell & & & \\ & & \ddots & & \\ & & & \ddots & \\ & & & & \ddots \end{bmatrix} [\Phi]^T \tag{85}$$

where $[\Phi]$ is a modal matrix which can be chosen as either one of the following two matrices;

$$\Phi_1 = \frac{1}{\sqrt{2N}} \begin{bmatrix} 1 & (e^{i\frac{2\pi}{2N}})^0 & (e^{-i\frac{2\pi}{2N}})^0 & \dots & \dots & (e^{-i\frac{2(N-1)\pi}{2N}})^0 & (e^{i\frac{2N\pi}{2N}})^0 \\ 1 & (e^{i\frac{2\pi}{2N}})^1 & (e^{-i\frac{2\pi}{2N}})^1 & \vdots & \vdots & (e^{-i\frac{2(N-1)\pi}{2N}})^1 & (e^{i\frac{2N\pi}{2N}})^1 \\ 1 & (e^{i\frac{2\pi}{2N}})^2 & (e^{-i\frac{2\pi}{2N}})^2 & \vdots & \vdots & (e^{-i\frac{2(N-1)\pi}{2N}})^2 & (e^{i\frac{2N\pi}{2N}})^2 \\ \vdots & \vdots & \vdots & \vdots & \vdots & \vdots & \vdots \\ 1 & (e^{i\frac{2\pi}{2N}})^{2N-2} & (e^{-i\frac{2\pi}{2N}})^{2N-2} & \vdots & \vdots & (e^{-i\frac{2(N-1)\pi}{2N}})^{2N-2} & (e^{i\frac{2N\pi}{2N}})^{2N-2} \\ 1 & (e^{i\frac{2\pi}{2N}})^{2N-1} & (e^{-i\frac{2\pi}{2N}})^{2N-1} & \dots & \dots & (e^{-i\frac{2(N-1)\pi}{2N}})^{2N-1} & (e^{i\frac{2N\pi}{2N}})^{2N-1} \end{bmatrix}_{2N \times 2N} \tag{86}$$

$\Phi_2 =$

$$\frac{1}{\sqrt{2N}} \begin{bmatrix} 1 & 1 & 0 & \dots & \dots & 0 & 1 \\ 1 & \cos(\frac{2\pi}{2N}) & \sin(\frac{2\pi}{2N}) & \vdots & \vdots & \sin(\frac{2\pi(N-1)}{2N}) & \cos(\frac{2\pi N}{2N}) \\ 1 & \cos(\frac{4\pi}{2N}) & \sin(\frac{4\pi}{2N}) & \vdots & \vdots & \sin(\frac{4\pi(N-1)}{2N}) & \cos(\frac{4\pi N}{2N}) \\ \vdots & \vdots & \vdots & \vdots & \vdots & \vdots & \vdots \\ 1 & \cos(\frac{2\pi(2N-2)}{2N}) & \sin(\frac{2\pi(2N-2)}{2N}) & \vdots & \vdots & \sin(\frac{\pi(4N-4)(N-1)}{2N}) & \cos(\frac{\pi(4N-4)(N)}{2N}) \\ 1 & \cos(\frac{2\pi(2N-1)}{2N}) & \sin(\frac{2\pi(2N-1)}{2N}) & \dots & \dots & \sin(\frac{\pi(4N-2)(N-1)}{2N}) & \cos(\frac{\pi(4N-2)(N)}{2N}) \end{bmatrix}_{2N \times 2N} \tag{87}$$

By substituting equations (84) and (85) into (83), we obtain

$$[C]^T[C] = [\Phi] \begin{bmatrix} \ddots & & & & \\ & (\lambda_\ell^2 + \mu_\ell^2) & & & \\ & & \ddots & & \\ & & & \ddots & \\ & & & & \ddots \end{bmatrix} [\Phi]^T. \tag{88}$$

Therefore, we have the singular values of $\sqrt{\lambda_\ell^2 + \mu_\ell^2}$, $\ell = 0, \pm 1, \dots, \pm(N - 1), N$. Only the true eigenvalues ($\lambda_\ell = \mu_\ell = 0$) have dips in the figure of σ_1 versus k , i.e., the zeros of eigensolutions ($J_\ell(k\rho) = 0$) are obtained for the Dirichlet problem.

For a circular cavity subject to the Neumann problem, we obtain the two eigenequations

$$\text{Single-layer approach : } J_i(k\rho)J'_i(k\rho) = 0 \quad (i \text{ no sum}),$$

$$\text{Double-layer approach : } J'_i(k\rho)J'_i(k\rho) = 0 \quad (i \text{ no sum}). \tag{89}$$

The true eigensolution $J'_i(k\rho) = 0$ satisfies both equations and the spurious eigensolutions $J_i(k\rho) = 0$ satisfies only one of equations in the single-layer potential approach for the Neumann problem. We can combine $[L^I]$ and $[M^I]$ matrices by using the updating terms to obtain an overdetermined system:

$$[C] = \begin{bmatrix} L^I \\ M^I \end{bmatrix}_{4N \times 2N} \tag{90}$$

for the Neumann problem. Since the eigensolution is non-trivial and the rank of $[C]$ must be smaller than $2N$. Therefore, the $2N$ singular values for $[C]$ matrix must have at least one zero value. Based on the equivalence between the SVD technique and the least-squares method in the mathematical essence, we have

$$\begin{bmatrix} [L^I]^T & [M^I]^T \end{bmatrix} \begin{bmatrix} [L^I] \\ [M^I] \end{bmatrix} = [L^I]^2 + [M^I]^2. \tag{91}$$

For the special case of a circular cavity of the Neumann problem, we can decompose $[L^I]$ and $[M^I]$ into

$$[L^I] = [\Phi] \begin{bmatrix} \ddots & & & & \\ & v_\ell & & & \\ & & \ddots & & \\ & & & \ddots & \\ & & & & \ddots \end{bmatrix} [\Phi]^T, \tag{92}$$

TABLE 5

The former five exact eigenvalues for a two-dimensional square cavity subject to the Dirichlet and Neumann boundary conditions

Problem	Eigenvalues	1	2	3	4	5
Dirichlet problem	$k_{mn} = \pi\sqrt{m^2 + n^2}$ ($m, n = 1, 2, 3, \dots$)	4.4429	7.0248	8.8858	9.9346	11.3271
Neumannproblem	$k_{mn} = \pi\sqrt{m^2 + n^2}$ ($m, n = 0, 1, 2, 3, \dots$)	3.1416	4.4429	6.2831	7.0248	8.8858

$$[M^I] = [\Phi] \begin{bmatrix} \ddots & & & & & \\ & \ddots & & & & \\ & & \kappa_\ell & & & \\ & & & \ddots & & \\ & & & & \ddots & \\ & & & & & \ddots \end{bmatrix} [\Phi]^T. \tag{93}$$

By substituting equations (92) and (91) into equation (91), we obtain

$$[C]^T[C] = [\Phi] \begin{bmatrix} \ddots & & & & & \\ & \ddots & & & & \\ & & (v_\ell^2 + \kappa_\ell^2) & & & \\ & & & \ddots & & \\ & & & & \ddots & \\ & & & & & \ddots \end{bmatrix} [\Phi]^T. \tag{94}$$

Therefore, we have the singular values of $\sqrt{v_\ell^2 + \kappa_\ell^2}$, $\ell = 0, \pm 1, \dots, \pm(N - 1), N$. Only the true eigenvalues ($v_\ell = \kappa_\ell = 0$) have dips in the figure of σ_1 versus k , i.e., the zeros of eigensolutions ($J'_\ell(k\rho) = 0$) are obtained for the Neumann problem.

7. METHOD TO FILTER OUT THE SPURIOUS EIGENSOLUTIONS

Fredholm’s Alternative Theorem

- (1) Nonsingular system: *The equation $[H]\{g\} = \{p\}$ has a unique solution $\{g\} = [H]^{-1}\{p\}$ when the determinant of H is not zero. Besides, the equation has a trivial solution $\{g\} = \{0\}$ if and only if the only continuous solution to the homogeneous equation $[H]\{g\} = \{0\}$.* (95)

- (2) Singular system: *Alternatively, the equation has at least one solution if the homogeneous adjoint equation has at least one solution $\{\phi_i\}$ such that*

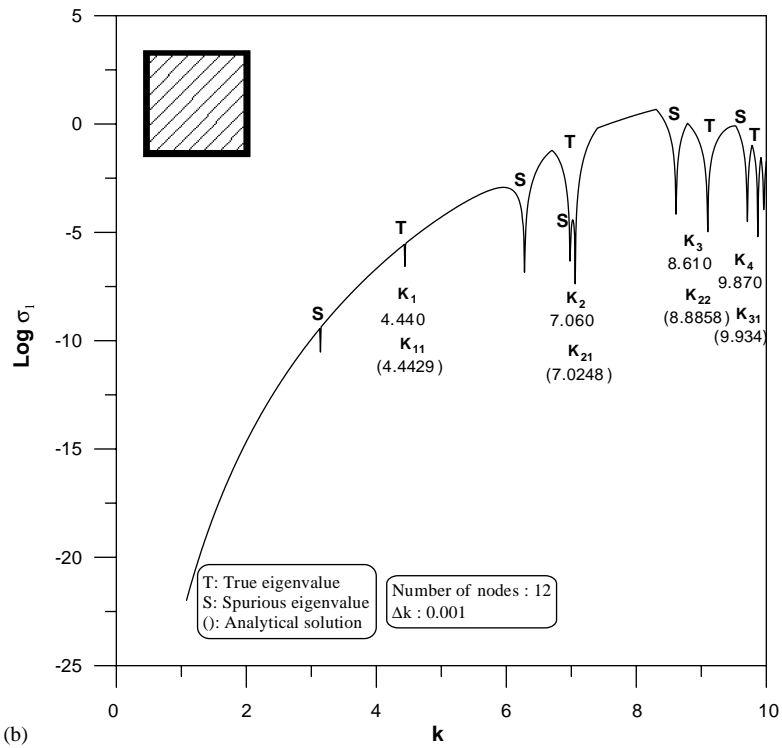
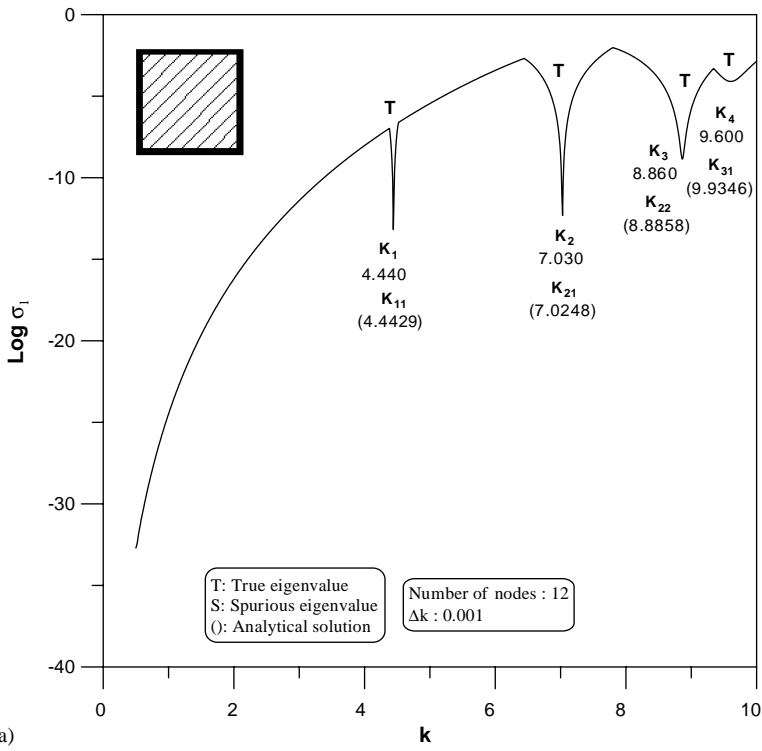
$$[H]^\dagger\{\phi_i\} = \{0\}, \tag{96}$$

where $[H]^\dagger$ is the transpose conjugate matrix of $[H]$ [24]. If the matrix H is real, the transpose conjugate is equal to transpose only, i.e., $[H]^\dagger = [H]^T$. Moreover, a necessary and sufficient solvability condition [25] is that the constraint $(\{p\})^\dagger\{\phi_i\} = 0$ must be satisfied. Then, the general solution can be written as

$$\{g\} = \{\bar{g}\} + \sum_{i=1}^{N_r} c_i \{\phi_i\}, \tag{97}$$

where $\{\bar{g}\}$ is a particular solution and N_r is the rank of matrix $[H]$. The c_i are arbitrary constants and $\{\phi_i\}$ are bases. Moreover, the particular solution is zero for the interior eigenproblems. The result implies that spurious eigenvalues are imbedded for both the Neumann and Dirichlet problems once the numerical method is chosen.

Figure 3. (a) The minimum singular value for different wave numbers by using the single-layer potential approach for the Dirichlet problem. (b) The minimum singular value for different wave numbers by using the double-layer potential approach for the Dirichlet problem. (c) The minimum singular value for different wave numbers by using the SVD updating term $[U \ T]$ for the Dirichlet problem. (d) The minimum singular value for different wave numbers by using the SVD updating document $[T \ M]$ for the Dirichlet problem. (e) The former three interior modes by using the single-layer potential approach for the Dirichlet problem. (f) The former three interior modes by using the double-layer potential approach for the Dirichlet problem. (g) The former three analytical interior modes for the Dirichlet problem.



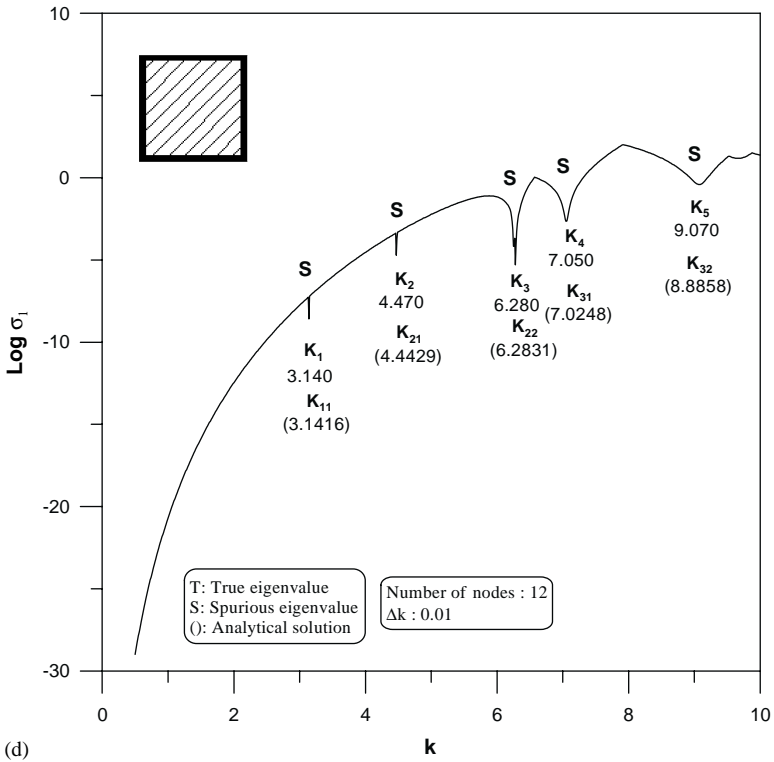
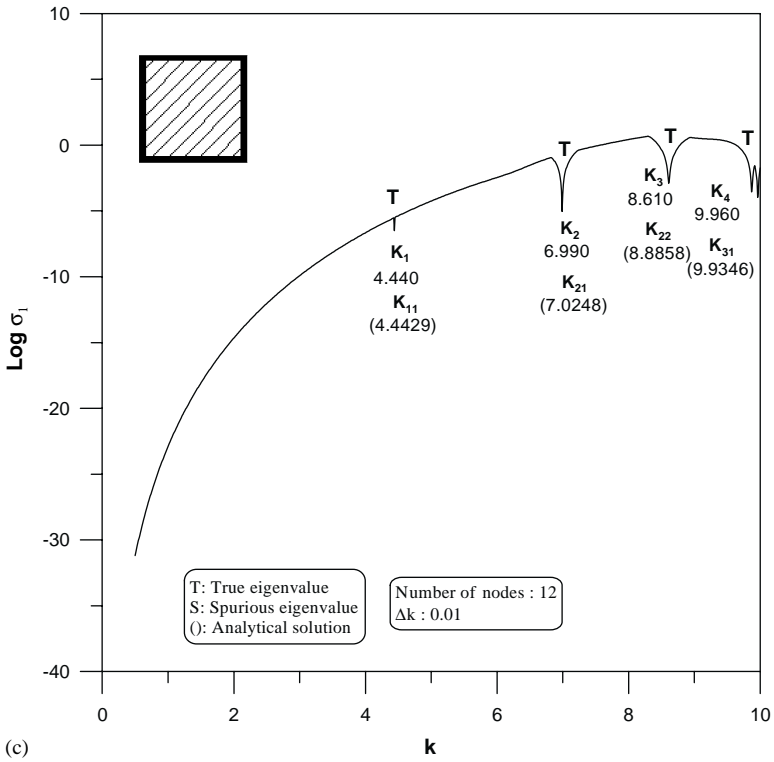


Figure 3. Continued.

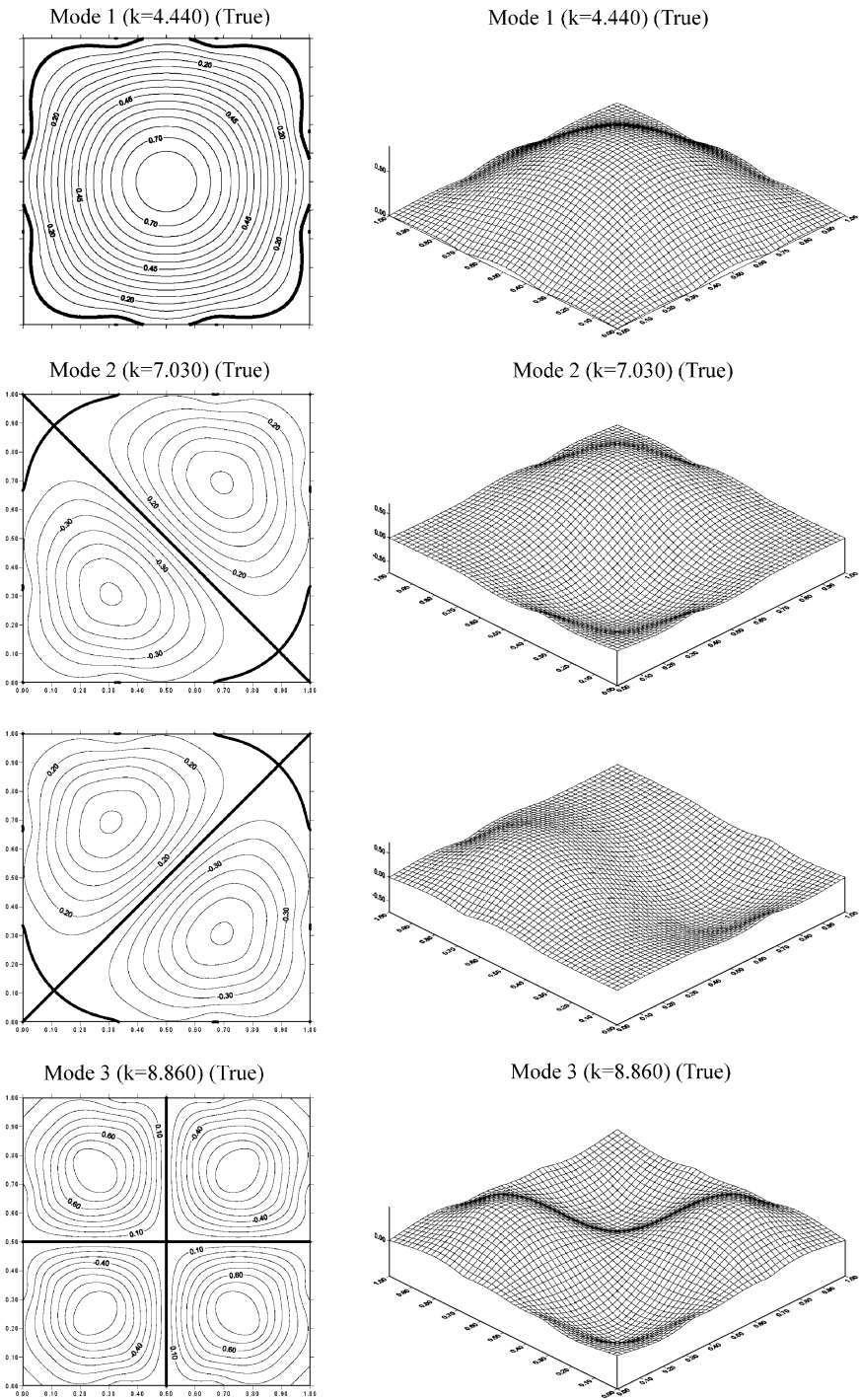
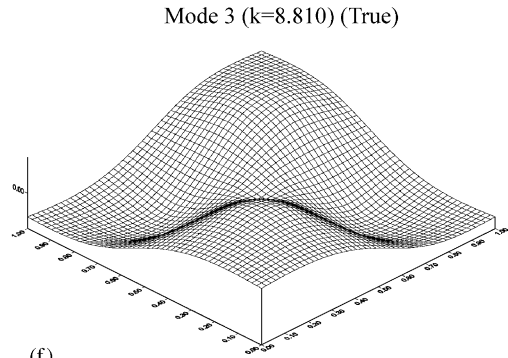
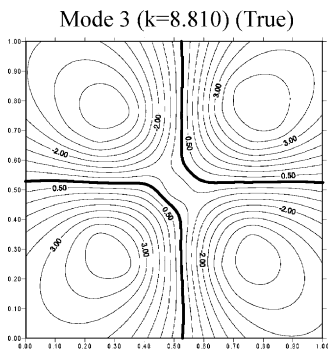
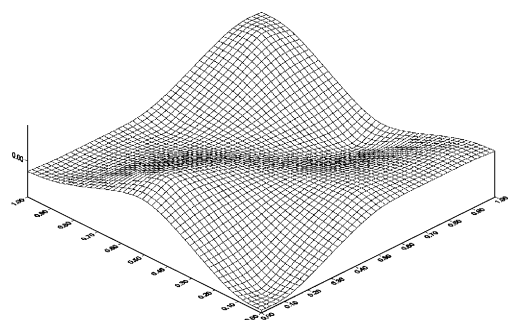
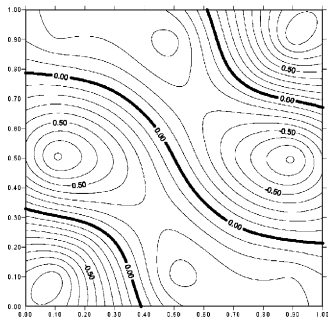
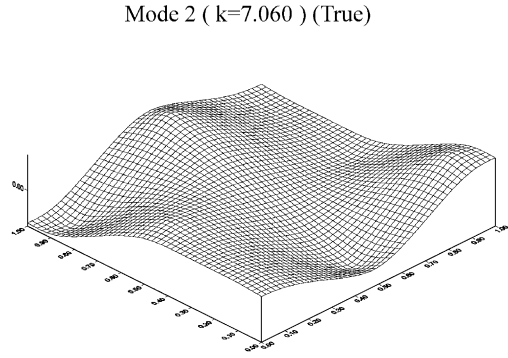
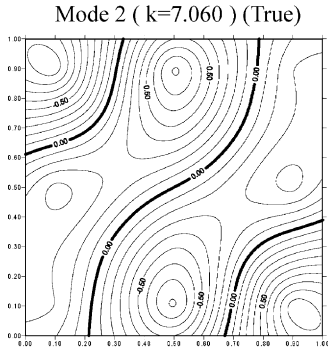
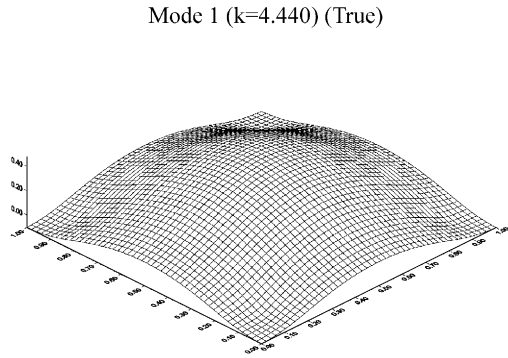
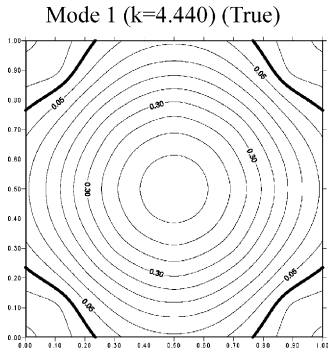
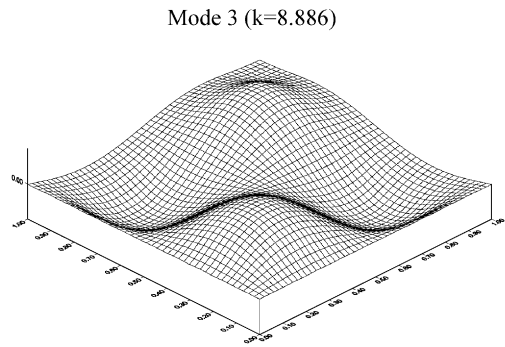
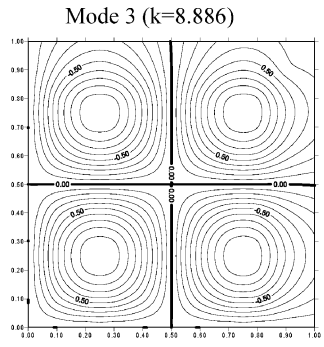
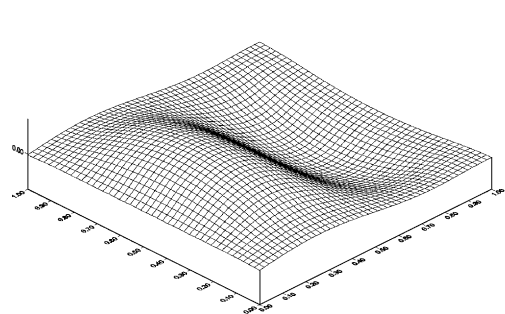
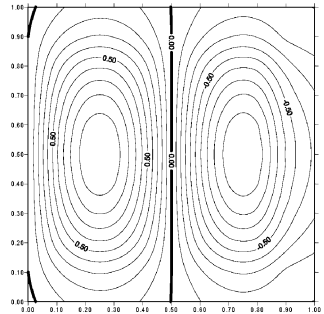
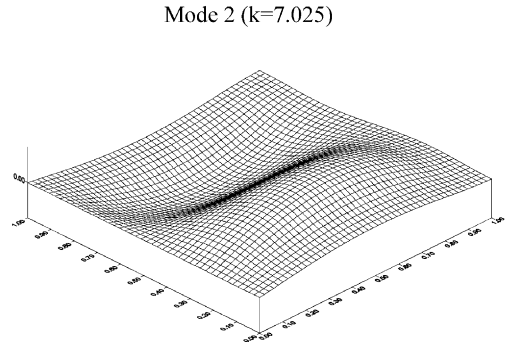
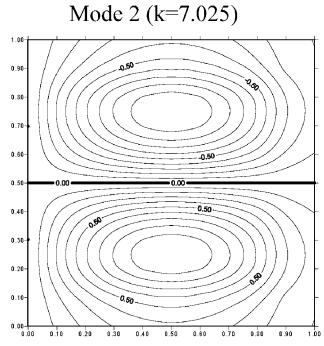
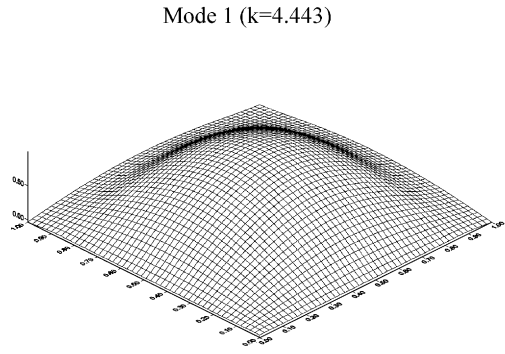
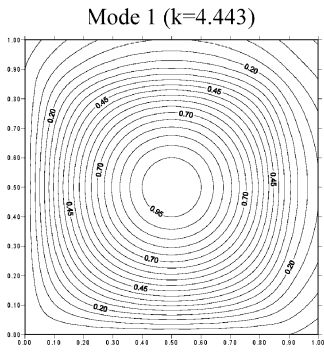


Figure 3. Continued.



(f)

Figure 3. Continued.



(g)

Figure 3. Continued.

By employing the LM formulation in the direct method, we have

$$\text{LM formulation: } [M^E] \{u\} = [L^E] \{t\} = \{p\}. \tag{98}$$

Hence the eigensolution for t is non-trivial, we have ϕ_i and $[L^E]^T \phi_i = \{0\}$ such that equation (98) reduces to

$$\{u^T\} [M^E]^T \{\phi_i\} = 0. \tag{99}$$

Since u is arbitrary for boundary excitation, we have

$$[M^E]^T \{\phi_i\} = \{0\}. \tag{100}$$

According to Fredholm’s alternative theorem in the real-matrix system, we have the homogeneous solutions in the linear algebraic equation if there exists a vector $\{\phi_i\}$ which satisfies

$$\begin{bmatrix} [L^E]^T \\ [M^E]^T \end{bmatrix} \{\phi_i\} = \{0\} \quad \text{or} \quad \{\phi_i\}^T \begin{bmatrix} [L^E] & [M^E] \end{bmatrix} = \{0\}. \tag{101}$$

It indicates that the two matrices have the same spurious mode $\{\phi_i\}$ corresponding to the zero singular value. By using the SVD technique, the two matrices in equation (101) are decomposed into

$$[L^E]^T = [\Psi^L][\Sigma^L][\Phi^L]^T \quad \text{or} \quad \{L_j^E\} = \sum_j \sigma_j^L \{\psi_j^L\} \{\phi_j^L\}^T, \tag{102}$$

$$[M^E]^T = [\Psi^M][\Sigma^M][\Phi^M]^T \quad \text{or} \quad \{M_j^E\} = \sum_j \sigma_j^M \{\psi_j^M\} \{\phi_j^M\}^T. \tag{103}$$

By substituting equation (103) into equation (101), we have

$$\begin{aligned} \sum_j \sigma_j^L \{\psi_j\} \{\phi_j\}^T \{\phi_i\} = \{0\} &\xrightarrow{\phi_i \cdot \phi_j = \delta_{ij}} \sigma_i^L \{\psi_i\} = \{0\} \quad (i \text{ no sum}), \\ \sum_j \sigma_j^M \{\psi_j\} \{\phi_j\}^T \{\phi_i\} = \{0\} &\xrightarrow{\phi_i \cdot \phi_j = \delta_{ij}} \sigma_i^M \{\psi_i\} = \{0\} \quad (i \text{ no sum}), \end{aligned} \tag{104}$$

where $\{\phi_i\}$ and $\{\psi_i\}$ are the orthonormal bases, σ_i^L and σ_i^M are the zero singular values of $[L^E]$ and $[M^E]$ matrices respectively. We can easily extract out the eigensolutions since there exists the same spurious boundary mode $\{\phi_i\}$ corresponding to the zero singular values ($\sigma_i^L = \sigma_i^M = 0$).

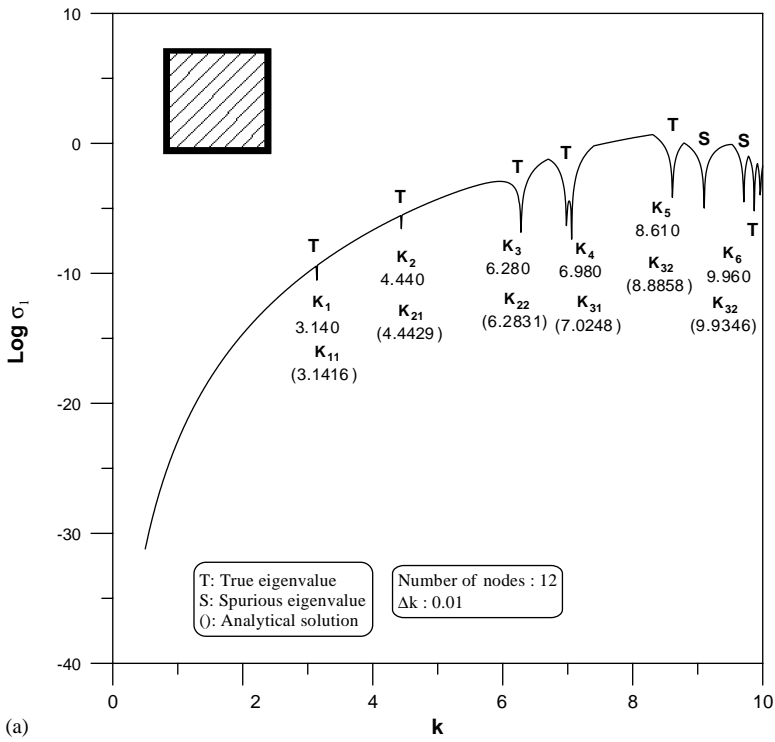
Similarly, we can employ the UT formulation in the direct method,

$$\text{UT formulation: } [U^E] \{t\} = [T^E] \{u\} = \{q\}. \tag{105}$$

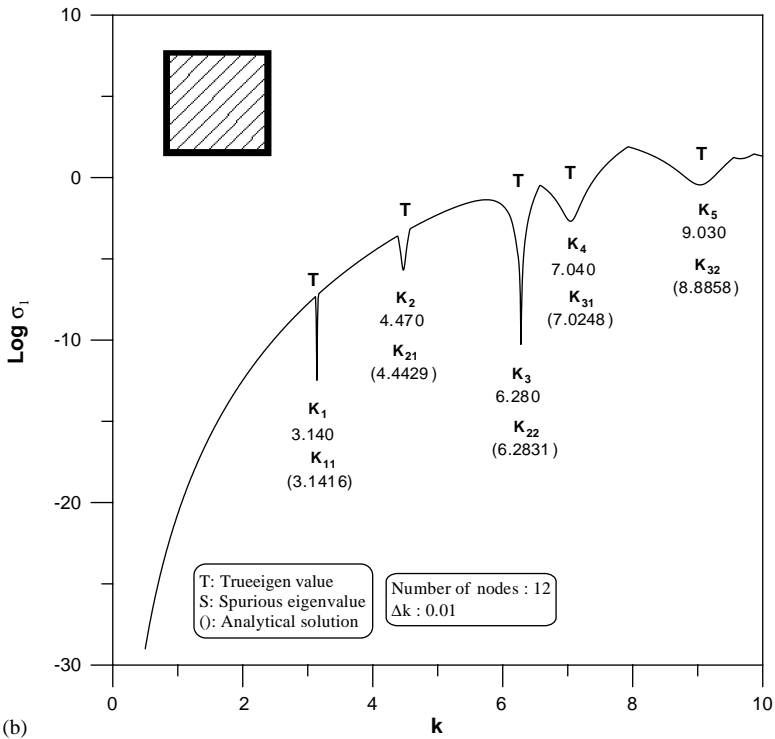
Since the eigensolution for u is non-trivial, we have ϕ_i and $[T^E]^T \phi_i = \{0\}$ such that equation (105) reduces to

$$\{t^T\} [U^E]^T \{\phi_i\} = 0. \tag{106}$$

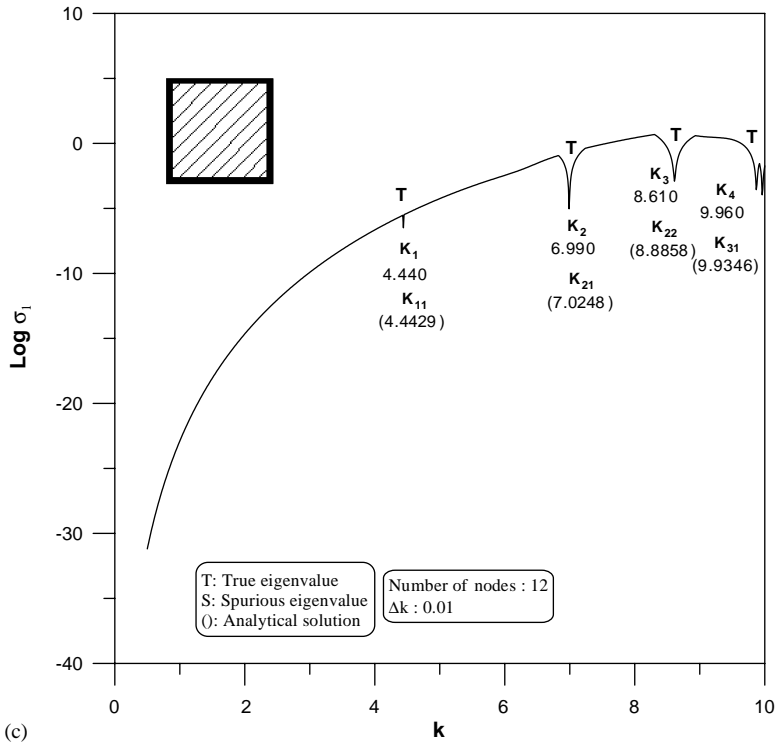
Figure 4. (a) The minimum singular value for different wave numbers by using the single-layer potential approach for the Neumann problem. (b) The minimum singular value for different wave numbers by using the double-layer potential approach for the Neumann problem. (c) The minimum singular value for different wave numbers using the SVD updating term $\begin{bmatrix} L & M \end{bmatrix}$ for the Neumann problem. (d) The minimum singular value for different wave numbers using the SVD updating document $\begin{bmatrix} U & L \end{bmatrix}$ for the Neumann problem. (e) The former three interior modes by using the single-layer potential approach for the Neumann problem. (f) The former three interior modes by using the double-layer potential approach for the Neumann problem. (g) The former three analytical interior modes for the Neumann problem.



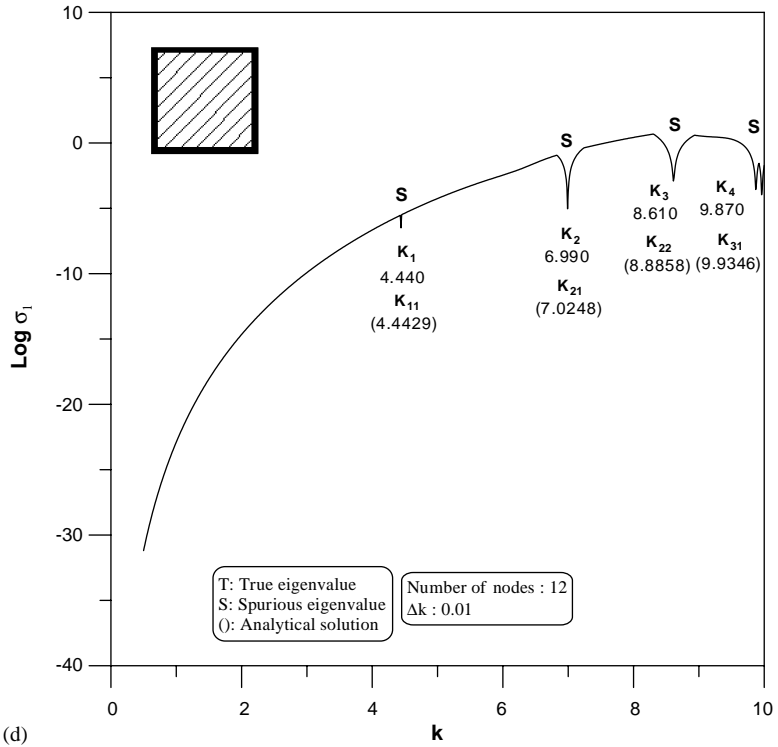
(a)



(b)



(c)



(d)

Figure 4. Continued.

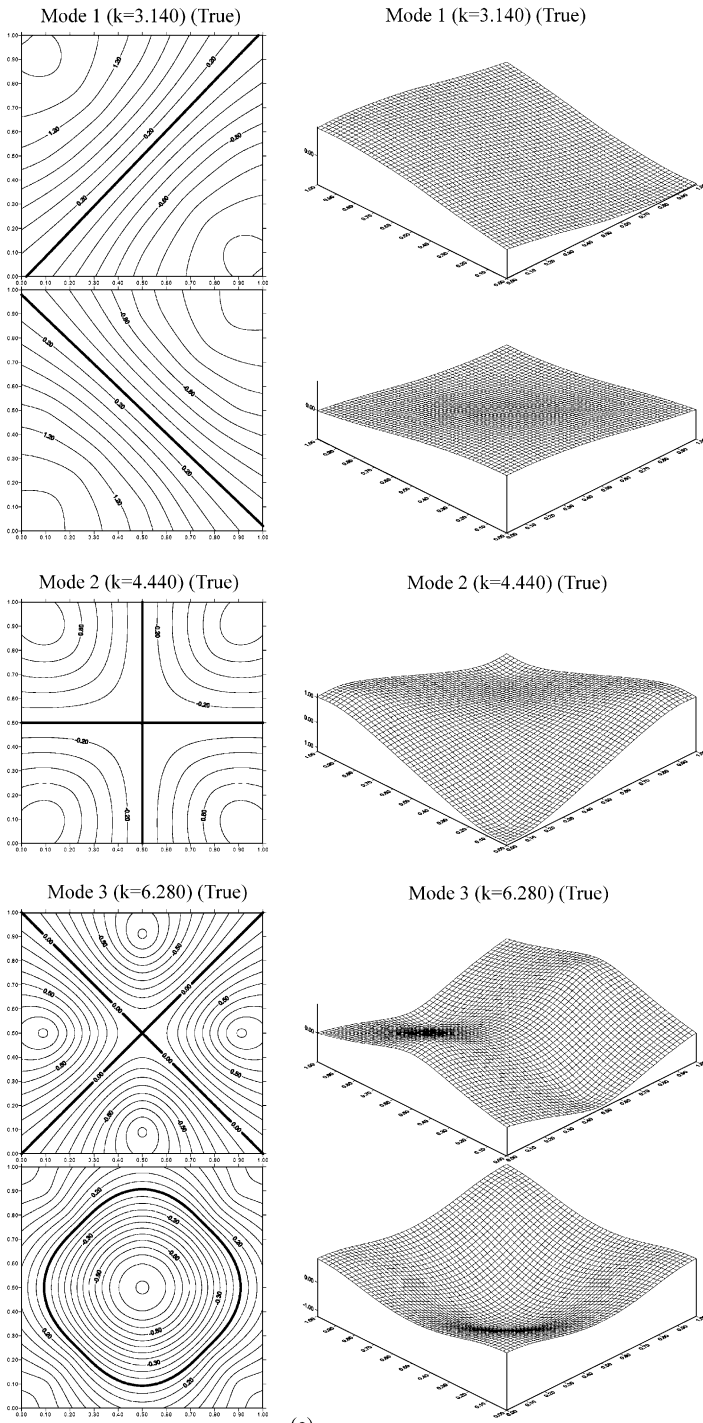
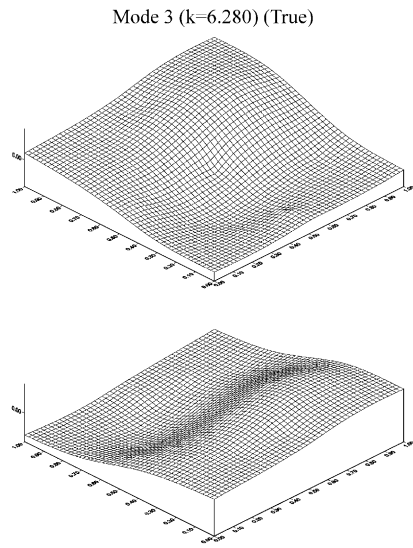
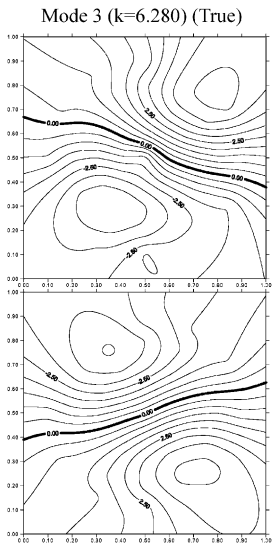
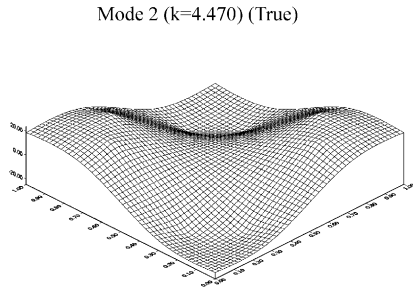
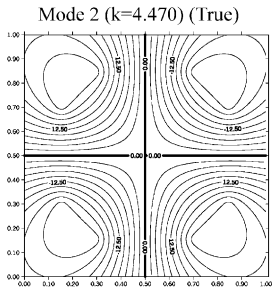
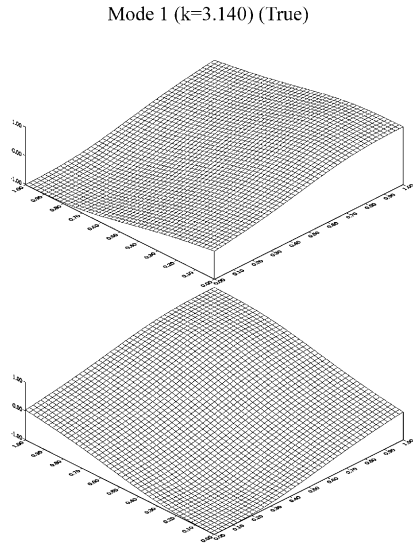
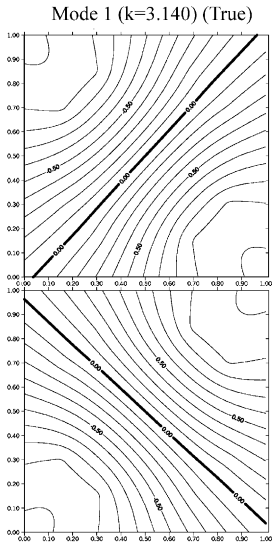


Figure 4. Continued.



(f)

Figure 4. Continued.

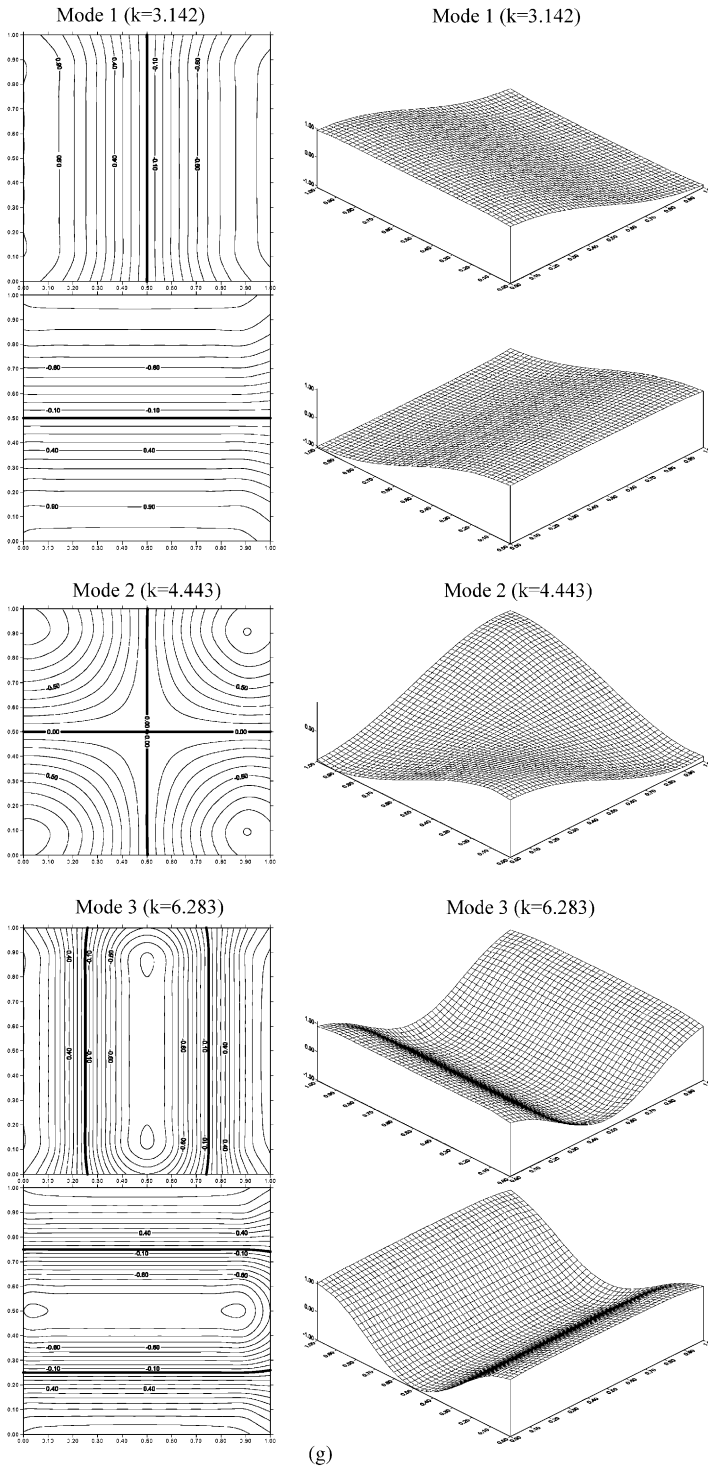


Figure 4. Continued.

Since $\{t\}$ is arbitrary for boundary excitation, we have

$$[U^E]^T \{\phi_i\} = \{0\}. \tag{107}$$

According to Fredholm’s alternative theorem, we have the homogeneous solutions in the linear algebraic equation if there exists a vector $\{\phi_i\}$ which satisfies

$$\begin{bmatrix} [U^E]^T \\ [T^E]^T \end{bmatrix} \{\phi_i\} = \{0\} \quad \text{or} \quad \{\phi_i\}^T \begin{bmatrix} [U^E] & [T^E] \end{bmatrix} = \{0\}. \tag{108}$$

It indicates that the two matrices have the same spurious boundary mode $\{\phi_i\}$ corresponding to the zero singular value. By using the SVD technique, equation (108) is expressed as

$$[U^E]^T = [\Psi][\Sigma^U][\Phi]^T, \tag{109}$$

$$[T^E]^T = [\Psi][\Sigma^T][\Phi]^T. \tag{110}$$

By substituting equation (110) into equation (108), we have

$$\begin{aligned} \sum_j \sigma_j^U \{\psi_j\} \{\phi_j\}^T \{\phi_i\} = \{0\} &\xrightarrow{\phi_i \cdot \phi_j = \delta_{ij}} \sigma_i^U \{\psi_i\} = \{0\} \quad (i \text{ no sum}), \\ \sum_j \sigma_j^T \{\psi_j\} \{\phi_j\}^T \{\phi_i\} = \{0\} &\xrightarrow{\phi_i \cdot \phi_j = \delta_{ij}} \sigma_i^T \{\psi_i\} = \{0\} \quad (i \text{ no sum}), \end{aligned} \tag{111}$$

where $\{\phi_i\}$ and $\{\psi_i\}$ are the orthonormal bases, σ_i^U and σ_i^T are the zero singular values of $[U^E]$ and $[T^E]$ matrices, respectively. We can easily extract out the eigensolutions since there exists the same spurious boundary mode $\{\phi_i\}$ corresponding to the zero singular values ($\sigma_i^U = \sigma_i^T = 0$).

According to the relations of the matrices between the direct method and indirect method (equations (49)–(52)), we can filter out the spurious eigensolutions in the indirect method by using

$$\begin{bmatrix} [L^E]^T \\ [M^E]^T \end{bmatrix} \{\phi_i\} = \{0\} \xrightarrow{\frac{L^E=T^I}{M^E=M^I}} \begin{bmatrix} [T^I]^T \\ [M^I]^T \end{bmatrix} \{\phi_i\} = \{0\}. \tag{112}$$

By employing the SVD technique, we obtain

$$\begin{aligned} \sum_j \sigma_j^T \{\psi_j\} \{\phi_j\}^T \{\phi_i\} = \{0\} &\xrightarrow{\phi_i \cdot \phi_j = \delta_{ij}} \sigma_i^T \{\psi_i\} = \{0\} \quad (i \text{ no sum}), \\ \sum_j \sigma_j^M \{\psi_j\} \{\phi_j\}^T \{\phi_i\} = \{0\} &\xrightarrow{\phi_i \cdot \phi_j = \delta_{ij}} \sigma_i^M \{\psi_i\} = \{0\} \quad (i \text{ no sum}), \end{aligned} \tag{113}$$

where $\{\phi_i\}$ and $\{\psi_i\}$ are the orthonormal bases, σ_i^T and σ_i^M are the zero singular values of $[T^I]$ and $[M^I]$ matrices, respectively. We can easily extract out the eigensolutions since there exists the same spurious boundary mode $\{\phi_i\}$ corresponding to the zero singular values ($\sigma_i^T = \sigma_i^M = 0$).

In a similar way, we have the influence matrices by using the indirect method and equation (108) is transformed to

$$\begin{bmatrix} [U^E]^T \\ [T^E]^T \end{bmatrix} \{\phi_i\} = \{0\} \xrightarrow{\frac{U^E=U^I}{T^E=I^I}} \begin{bmatrix} [U^I]^T \\ [L^I]^T \end{bmatrix} \{\phi_i\} = \{0\}. \tag{114}$$

By using the SVD technique, we obtain

$$\sum_j \sigma_j^U \{\psi_j\} \{\phi_j\}^T \{\phi_i\} = \{0\} \xrightarrow{\phi_i \cdot \phi_j = \delta_{ij}} \sigma_i^U \{\psi_i\} = \{0\} \quad (i \text{ no sum}),$$

$$\sum_j \sigma_j^L \{\psi_j\} \{\phi_j\}^T \{\phi_i\} = \{0\} \xrightarrow{\phi_i \cdot \phi_j = \delta_{ij}} \sigma_i^L \{\psi_i\} = \{0\} \quad (i \text{ no sum}), \tag{115}$$

where $\{\phi_i\}$ and $\{\psi_i\}$ are the orthonormal bases, σ_i^U and σ_i^L are the singular values of $[U^I]$ and $[L^I]$ matrices, respectively. We can easily extract out the eigensolutions since there exists the same spurious boundary mode $\{\phi_i\}$ corresponding to the zero singular values ($\sigma_i^U = \sigma_i^L = 0$).

7.1. FILTERING OUT THE SPURIOUS EIGENSOLUTIONS BY USING SVD UPDATING DOCUMENT FOR A CIRCULAR CASE

In solving a circular cavity problem using the double-layer potential approach, we obtain the eigenequations

$$\text{Dirichlet problem : } J_i(k\rho)J'_i(k\rho) = 0 \quad (i \text{ no sum}), \tag{116}$$

$$\text{Neumann problem : } J'_i(k\rho)J'_i(k\rho) = 0 \quad (i \text{ no sum}). \tag{117}$$

The spurious eigensolution $J'_i(k\rho)$ are embedded in both the Dirichlet and the Neumann problems.

Based on the dual formulation, the $[T^I]$ and $[M^I]$ matrices have the same spurious eigenvalues. In order to extract the spurious eigenvalues, we can combine the $[T^I]$ and $[M^I]$ matrices by using the updating documents,

$$[D] = \begin{bmatrix} [T^I] & [M^I] \end{bmatrix}_{2N \times 4N}. \tag{118}$$

Similarly, we have

$$\begin{bmatrix} [T^I] & [M^I] \end{bmatrix} \begin{bmatrix} [T^I]^T \\ [M^I]^T \end{bmatrix} = [T^I]^2 + [M^I]^2. \tag{119}$$

For the circular cavity, the spurious eigenvalues are both embedded in the transposes of $[T^I]$ and $[M^I]$ matrices according to equations (11)–(14). The singular values for $[D]$ must have at least one zero singular value. To determine the singular values for $[D]$, we have

$$[D][D]^T = [\Phi] \begin{bmatrix} \ddots & & & \\ & (\mu_\ell^2 + \kappa_\ell^2) & & \\ & & \ddots & \\ & & & \ddots \end{bmatrix} [\Phi]^T. \tag{120}$$

By plotting the minimum singular values of $\sqrt{\mu_\ell^2 + \kappa_\ell^2}$, $\ell = 0, \pm 1, \dots, \pm(N - 1), N$ versus k , we can filter out the spurious eigenvalues ($\nu_\ell = \kappa_\ell = 0$) where dips occur, i.e., the zeros of eigensolutions ($J'_\ell(k\rho) = 0$) are obtained by using the double-layer potential approach.

In solving a circular cavity by using the single-layer potential approach, we obtain

$$\text{Dirichlet problem: } J_i(k\rho)J_i(k\rho) = 0 \quad (i \text{ no sum}), \tag{121}$$

$$\text{Neumann problem: } J_i(k\rho)J'_i(k\rho) = 0 \quad (i \text{ no sum}). \tag{122}$$

The spurious eigensolution $J_i(k\rho)$ are embedded in both the Dirichlet and the Neumann problems.

In a similar way, we can combine the $[U^I]$ and $[L^I]$ matrices by using the updating documents,

$$[D] = \begin{bmatrix} [U^I] & [L^I] \end{bmatrix}_{2N \times 4N}. \tag{123}$$

Similarly, we have

$$\begin{bmatrix} [U^I] & [L^I] \end{bmatrix} \begin{bmatrix} [U^I] & [L^I] \end{bmatrix}^T = [U^I]^2 + [L^I]^2. \tag{124}$$

For the special case of a circular cavity, the spurious eigenvalues are embedded in the transpose of $[U^I]$ and $[L^I]$ matrices according to equations (11)–(14). The singular values for $[D]$ must have at least one zero singular value. To determine the singular values for $[D]$, we have

$$[D][D]^T = [\Phi] \begin{bmatrix} \ddots & & & \\ & (\lambda_\ell^2 + \nu_\ell^2) & & \\ & & \ddots & \\ & & & \ddots \end{bmatrix} [\Phi]^T. \tag{125}$$

By plotting the minimum singular values of $\sqrt{\lambda_\ell^2 + \nu_\ell^2}$, $\ell = 0, \pm 1, \dots, \pm(N - 1), N$ versus k , we can filter out the spurious eigenvalues ($\lambda_\ell = \nu_\ell = 0$) where dips occur, i.e., the zeros of eigensolutions ($J_\ell(k\rho) = 0$) are obtained.

All the relations between the direct and indirect methods are shown in Table 2. We can easily extract out the true and spurious eigenvalues in the indirect method or the direct method by using the SVD updating terms and documents.

8. NUMERICAL RESULTS AND DISCUSSIONS

Case 1: Circular cavity (Dirichlet case). A circular cavity with a radius ($\rho = 1$ m) subjected to the Dirichlet boundary condition ($u = 0$) is considered. In this case, an analytical solution is available as follows:

Eigenequation:

$$J_m(k_n\rho) = 0, \quad m, n = 0, 1, 2, 3, \dots$$

Eigenmode:

$$u(a, \theta) = J_m(k_n a) e^{im\theta}, \quad 0 \leq a \leq \rho, \quad 0 \leq \theta \leq 2\pi, \quad m, n = 0, 1, 2, 3, \dots$$

By collocating 10 nodes on the circular boundary, two results by using the single- and double-layer potential approaches are obtained. The exact eigenvalues of a circular cavity subject to the Dirichlet boundary condition are shown in Table 3. Figure 1(a) shows the minimum singular value versus k using the single-layer potential approach. The former four true eigenvalues are obtained as shown in Figure 1(a) by considering the near zero minimum singular values if only the single-layer potential method is chosen. Figure 1(b) shows the minimum singular value versus k using the double-layer potential approach. The true eigenvalues occur at the positions of zeros for $J_m(k_n\rho)$ while the spurious eigenvalues occur at the positions of zeros for $J'_m(k_n\rho)$ if the double-layer approach is chosen. In order to extract out the true eigenvalues, we can combine the $[U^I]$ and $[T^I]$ by using the SVD updating term. The minimum singular value versus k is shown in Figure 1(c), it is found that dips occur only at the positions of true eigenvalues. In a similar way, we can combine the $[T^I]$ and $[M^I]$ by using the SVD updating document in order to filter

out the spurious eigenvalues. The minimum singular value versus k is shown in Figure 1(d), it is found that the dips occur only at the positions of spurious eigenvalues. The first three interior modes obtained by using the single- and double-layer potential approaches are shown in Figures 1(e) and 1(f), and are compared well with the analytical modes in Figure 1(g). It is observed that the nodal line can rotate in case of the eigenvalue of multiplicity more than one. There are two independent eigenmodes with respect to the same eigenvalue. The two modes can be linearly combined by any constants and can differ by the phase lag. This is the reason why the one mode can be rotated to another mode. A similar explanation can also be found in Reference [26]. It is also found that the result of case 1 in Figure 1(e) does not match the analytical solution very well. The reason is that the amplitudes of the modes are very small since they are multiplied by a near-zero value. However, the nodal line can be identified. To demonstrate this point, the exact solutions for the mode using the present method are shown to have the near-zero solutions in Table 4. The near-zero solutions are present if the single-layer approach was applied to solve the Dirichlet problem.

Case 2: Circular cavity (Neumann case). A circular cavity with a radius ($\rho = 1$ m) subjected to the Neumann boundary condition ($t = 0$) is considered. In this case, an analytical solution is available as follows:

Eigenequation:

$$J'_m(k_n \rho) = 0, \quad m, n = 0, 1, 2, 3, \dots$$

Eigenmode:

$$u(a, \theta) = J_m(k_n a) e^{im\theta}, \quad 0 \leq a \leq \rho, \quad 0 \leq \theta \leq 2\pi, \quad m, n = 0, 1, 2, 3, \dots$$

By collocating 10 nodes on the circular boundary, two results by using the single- and double-layer potential approaches are obtained. The exact eigenvalues of a circular cavity subject to the Neumann boundary condition are shown in Table 3. Figure 2(a) shows the minimum singular value versus k using the single-layer potential approach. The former four true eigenvalues are obtained as shown in Figure 2(a) by considering the near-zero minimum singular values if only the single-layer potential method is chosen. Figure 2(b) shows the minimum singular value versus k using the double-layer potential approach. The true eigenvalues occur at the positions of zeros for $J'_m(k_n \rho)$ while the spurious eigenvalues occur at the positions of zeros for $J_m(k_n \rho)$ if the double-layer approach is chosen. In order to extract out the true eigenvalues, we combine the $[L^I]$ and $[M^I]$ by using the SVD updating term. The minimum singular value versus k is shown in Figure 2(c), it is found that the dips occur only at the positions of true eigenvalues. In a similar way, we combine the $[U^I]$ and $[L^I]$ by using the SVD updating document in order to filter out the spurious eigenvalues. The minimum singular value versus k is shown in Figure 2(d), it is found that the dips occur only at the positions of spurious eigenvalues. The first three interior modes obtained by using the single- and double-layer potential approaches are shown in Figure 2(e) and Figure 2(f), and are compared well with the analytical modes in Figure 2(g) for the nodal lines. It is found that the nodal line can rotate in case of the eigenvalue of multiplicity more than one. There are two independent eigenmodes with respect to the same eigenvalue. The two modes can be linearly combined by any constants and can differ by the phase lag. This is the reason why the one mode can be rotated to another mode. A similar explanation can also be found in Reference [26]. It is also found that the result of case 2 in Figure 2(f) does not match the analytical solution very well. The reason is that the amplitudes of the modes are very small since they are multiplied by a near-zero value. However, the nodal line can be identified. To demonstrate this point, the exact solutions for the mode using the present method are shown to have the near-zero

solutions in Table 4. The near-zero solutions are present if the double-layer approach was applied to solve the Neumann problem.

Case 3: Square cavity (Dirichlet case). A square cavity with each side of a unit length ($L = 1$) subjected to the Dirichlet boundary condition ($u = 0$) is considered. In this case, an analytical solution is available as follows:

Eigenvalues:

$$k_{mn} = \sqrt{\left(\frac{m}{L}\right)^2 + \left(\frac{n}{L}\right)^2} \pi, \quad m, n = 1, 2, 3, \dots$$

Eigenmode:

$$\sin\left(\frac{m\pi x}{L}\right) \sin\left(\frac{n\pi x}{L}\right), \quad m, n = 1, 2, 3, \dots$$

By collocating 12 nodes on the boundary, two results by using the single- and double-layer potential approaches are obtained. The exact eigenvalues of a square cavity subject to the Dirichlet boundary condition are shown in Table 5. Figure 3(a) shows the minimum singular value versus k using the single-layer potential approach. The former four true eigenvalues are obtained as shown in Figure 3(a) by considering the near-zero minimum singular values if only the single-layer potential method is chosen. Figure 3(b) shows the minimum singular value versus k using the double-layer potential approach. The true eigenvalues occur at the positions of $k_{mn} = \sqrt{(m/L)^2 + (n/L)^2}$ while the spurious eigenvalues occur if the double-layer approach is chosen. In order to extract out the true eigenvalues, we combine the $[U^I]$ and $[T^I]$ by using the SVD updating term. The minimum singular value versus k is shown in Figure 3(c), it is found that the dips occur only at the positions of true eigenvalues. In a similar way, we combine the $[T^I]$ and $[M^I]$ by using the SVD updating document in order to filter out the spurious eigenvalues. The minimum singular value versus k is shown in Figure 3(d), it is found that the dips occur only at the positions of spurious eigenvalues. The first three interior modes using the single- and double-layer approaches are shown in Figure 3(e) and Figure 3(f) and are compared with analytical modes in Figure 3(g). For the eigenvalue of multiplicity more than one, some discrepancy for the nodal line is found since the eigensolution can be superimposed by two independent eigensolutions of the same eigenvalue.

Case 4: Square cavity (Neumann case). A square cavity with each side of a unit length ($L = 1$) subjected to the Neumann boundary condition ($t = 0$) is considered. In this case, an analytical solution is available as follows:

Eigenvalues:

$$k_{nm} = \sqrt{\left(\frac{m}{L}\right)^2 + \left(\frac{n}{L}\right)^2} \pi, \quad m, n = 0, 1, 2, 3, \dots$$

Eigenmode:

$$\cos\left(\frac{m\pi x}{L}\right) \cos\left(\frac{n\pi x}{L}\right), \quad m, n = 0, 1, 2, 3, \dots$$

By collocating 12 nodes on the boundary, two results by using the single- and double-layer approaches are obtained. The exact eigenvalues of a square cavity subject to the Neumann boundary condition are shown in Table 5. Figure 4(a) shows the minimum singular value versus k using the single-layer potential approach. The former four true eigenvalues are obtained as shown in Figure 4(a) by considering the near-zero minimum singular values if only the single-layer potential method is chosen. Figure 4(b) shows the minimum singular value versus k using the double-layer potential approach. The true

TABLE 6

The true and spurious eigenvalues for circular and square cavities using the single- and double-layer potential approaches

Boundary-value problem	Eigensolution	Circular cavity		Square cavity	
		Single-layer potential approach	Double-layer potential approach	Single-layer potential approach	Double-layer potential approach
Dirichlet problem	True eigensolution	$J_m(k\rho) = 0$	$J_m(k\rho) = 0$	$k_{mn} = \sqrt{\left(\frac{m}{L}\right)^2 + \left(\frac{n}{L}\right)^2} \pi$	$k_{mn} = \sqrt{\left(\frac{m}{L}\right)^2 + \left(\frac{n}{L}\right)^2} \pi$
		(Figure 1(a))	(Figure 1(b))	$(m, n = 1, 2, 3, \dots)$ (Figure 3(a))	$(m, n = 1, 2, 3, \dots)$ (Figure 3(b))
	Spurious eigensolution	$J_m(k\rho) = 0$	$J'_m(k\rho) = 0$	$k_{mn} = \sqrt{\left(\frac{m}{L}\right)^2 + \left(\frac{n}{L}\right)^2} \pi$	$k_{mn} = \sqrt{\left(\frac{m}{L}\right)^2 + \left(\frac{n}{L}\right)^2} \pi$
		(Figure 1(a))	(Figure 1(b))	$(m, n = 1, 2, 3, \dots)$ (Figure 3(a))	$m, n = 0, 1, 2, 3, \dots)$ (Figure 3(b))
Neumann problem	True eigensolution	$J'_m(k\rho) = 0$	$J'_m(k\rho) = 0$	$k_{mn} = \sqrt{\left(\frac{m}{L}\right)^2 + \left(\frac{n}{L}\right)^2} \pi$	$k_{mn} = \sqrt{\left(\frac{m}{L}\right)^2 + \left(\frac{n}{L}\right)^2} \pi$
		(Figure 2(a))	(Figure 2(b))	$(m, n = 0, 1, 2, 3, \dots)$ (Figure 4(a))	$m, n = 0, 1, 2, 3, \dots)$ (Figure 4(b))
	Spurious eigensolution	$J_m(k\rho) = 0$	$J'_m(k\rho) = 0$	$k_{mn} = \sqrt{\left(\frac{m}{L}\right)^2 + \left(\frac{n}{L}\right)^2} \pi$	$k_{mn} = \sqrt{\left(\frac{m}{L}\right)^2 + \left(\frac{n}{L}\right)^2} \pi$
		(Figure 2(a))	(Figure 2(b))	$(m, n = 1, 2, 3, \dots)$ (Figure 4(a))	$(m, n = 0, 1, 2, 3, \dots)$ (Figure 4(b))

eigenvalues occur at the positions of $k_{mn} = \sqrt{(m/L)^2 + (n/L)^2}$ while the spurious eigenvalues occur if the double-layer approach is chosen. In order to extract out the true eigenvalues, we combine the $[L^I]$ and $[M^I]$ by using the SVD updating term. The minimum singular value versus k is shown in Figure 4(c), it is found that the dips occur only at the positions of true eigenvalues. In a similar way, we combine the $[U^I]$ and $[L^I]$ by using the SVD updating document in order to filter out the spurious eigenvalues. The minimum singular value versus k is shown in Figure 4(d), it is found that the dips occur only at the positions of spurious eigenvalues. The former three interior modes for the single- and double-layer potential approaches are shown in Figure 4(e) and Figure 4(f), and are compared with the analytical modes in Figure 4(g). For the eigenvalue of multiplicity more than one, some discrepancy for the nodal line is found since the eigensolution can be superimposed by two independent eigensolutions of the same eigenvalue.

9. CONCLUSIONS

We have developed a new meshless method by using the imaginary-part kernel. The imaginary part in the complex-valued fundamental solution was chosen as a radial basis function to approximate the solution. Although this method is very simple by using only two-point function for the influence matrices, it results in spurious eigensolutions as shown in Table 6. Two approaches, the SVD updating terms and updating documents in conjunction with dual formulation, were proposed to extract out the true eigensolutions and to filter out the spurious eigensolutions, respectively, as shown in Table 2. Both cases, circular and square cavities, subject to the Dirichlet and the Neumann boundary conditions, were demonstrated to check the validity of the meshless formulation.

ACKNOWLEDGMENTS

Financial support from the National Science Council under Grant No. NSC-90-2211-E-019-006 for National Taiwan Ocean University is gratefully acknowledged.

REFERENCES

1. R. A. GINGOLD and J. J. MARAGHAN 1977 *Monthly Notices of the Royal Astronomical Society* **181**, 375–389. Smoothed particle hydrodynamics: theory and applications to non-spherical stars.
2. P. LANCASTER and K. SALKAUSKAS 1981 *Mathematics of Computation* **37**, 141–158. Surfaces generated by moving least-squares methods.
3. W. K. LIU, S. JUN, S. LI, J. ADEE and T. BELYSCHKO 1995 *International Journal for Numerical Methods in Engineering* **38**, 1655–1679. Reproducing kernel particle methods for structural dynamics.
4. W. YEIH, J. T. CHEN, K. H. CHEN and F. C. WONG 1998 *Advances in Engineering Software* **29**, 7–12. A study on the multiple reciprocity method and complex-valued formulation for the Helmholtz equation.
5. J. T. CHEN, C. X. HUANG and K. H. CHEN 1999 *Computational Mechanics* **24**, 41–51. Determination of spurious eigenvalues and multiplicities of true eigenvalues using the real-part dual BEM.
6. J. T. CHEN and F. C. WONG 1997 *Engineering Analysis with Boundary Elements* **20**, 25–33. Analytical derivations for one-dimensional eigenproblems using dual BEM and MRM.
7. J. T. CHEN and F. C. WONG 1998 *Journal of Sound and Vibration* **217**, 75–95. Dual formulation of multiple reciprocity method for the acoustic mode of a cavity with a thin partition.

8. S. R. KUO, J. T. CHEN and C. X. HUANG 2000 *International Journal for Numerical Methods in Engineering* **48**, 1401–1422. Analytical study and numerical experiments for true and spurious eigenolutions of a circular cavity using the real-part dual BEM.
9. N. KAMIYA, E. ANDO and K. NOGAE 1996 *Advances in Engineering Software* **26**, 219–227. A new complex-valued formulation and eigenvalue analysis of the Helmholtz equation by boundary element method.
10. D. Y. LIU, J. T. CHEN and K. H. CHEN 1999 *Journal of the Chinese Institute of Civil Hydrogen Engineering* **11**, 89–100. A new method for determining the acoustic modes of a two-dimensional sound field. (in Chinese)
11. G. R. G. TAI and R. P. SHAW 1974 *Journal of the Acoustical Society of America* **56**, 796–804. Helmholtz equation eigenvalues and eigenmodes for arbitrary domains.
12. A. J. NOWAK and A. C. NEVES, editors 1994 *Multiple Reciprocity Boundary Element Method*. Southampton: Comp. Mech. Publ.
13. G. DE MEY 1977 *Journal of the Acoustical Society of America* **11**, 1340–1342. A simplified integral equation method for the calculation of the eigenvalues of Helmholtz equation.
14. S. W. KANG and J. M. LEE 2000 *Journal of Sound and Vibration* **234**, 455–470. Application of free vibration analysis of membranes using the non-dimensional dynamic influence function.
15. S. W. KANG, J. M. LEE and Y. J. KANG 1999 *Journal of Sound and Vibration* **221**, 117–132. Vibration analysis of arbitrary shaped membranes using non-dimensional dynamic influence function.
16. S. W. KANG and J. M. LEE 2000 *Journal of the Acoustical Society of America* **234**, 1153–1160. Eigenmode analysis of arbitrarily shaped two-dimensional cavities by the method of point-matching.
17. J. T. CHEN, S. R. KUO, K. H. CHEN and Y. C. CHENG 2000 *Journal of Sound and Vibration* **235**, 156–171. Comments on “Vibration analysis of arbitrary shaped membranes using non-dimensional dynamic influence function”.
18. J. T. CHEN, C. X. HUANG and F. C. WONG 2000 *Journal of Sound and Vibration* **230**, 219–230. Determination of spurious eigenvalues and multiplicities of true eigenvalues in the dual multiple reciprocity method using the singular value decomposition technique.
19. J. T. CHEN, M. H. CHANG, I. L. CHUNG and Y. C. CHENG 2002 *Journal of the Acoustical Society of America* **111**, 33–36. Comments on “Eigenmode analysis of arbitrarily shaped two-dimensional cavities by the method of point matching.”
20. G. H. GOLUB and C. F. VAN LOAN 1989 *Matrix Computations*. Baltimore: The Johns Hopkins University Press; second edition.
21. J. L. GOLDBERG 1991 *Matrix Theory with Applications*, New York: McGraw-Hill.
22. J. T. CHEN and H. K. HONG 1999 *Transactions of the American Society of Mechanical Engineers, Applied Mechanics Review* **52**, 17–33. Review of dual integral representations with emphasis on hypersingular integrals and divergent series.
23. J. T. CHEN and K. H. CHEN 1998 *Engineering Analysis with Boundary Elements* **21**, 105–116. Dual integral formulation for determining the acoustic modes of a two-dimensional cavity with a degenerate boundary.
24. H. T. DAVIS and K. T. THOMSON 2000 *Linear Algebra and Linear Operators in Engineering with Applications in Mathematica*, Vol. 3. New York: Academic Press.
25. I. STAKGOLD 1979 *Green's Functions and Boundary Value Problems*. New York: John Wiley & Sons.
26. J. T. CHEN, K. H. CHEN and S. W. CHYUAN 1999 *Applied Acoustics* **57**, 293–325. Numerical experiments for acoustic modes of a square cavity using the dual boundary element method.